Canadian Journal of Forest Research

Research Article

Linking burn severity to pre-fire forest structure and weather on the Dixie fire offers potential to map prospective burn severity

Thomas Estabrook[a], **Jeremy Fried**[b], **Weimin Xi**[a], **Haibin Su**[c], **and Jianwei Zhang**[d]

[a]Department of Biological and Health Sciences, Texas A&M University-Kingsville, Kingsville, TX 78363, USA; [b]United States Department of Agriculture Forest Service, Pacific Northwest Research Station, Portland, OR 97204, USA; [c]Department of Physics and Geosciences, Texas A&M University-Kingsville, Kingsville, TX 78363, USA; [d]United States Department of Agriculture Forest Service, Pacific Southwest Research Station, Redding, CA 96002, USA

Corresponding author: **Weimin Xi** (email: Weimin.Xi@tamuk.edu)

Abstract

Seeking to understand controllable stand structure drivers of high burn severity, contingent on weather, 35 candidate predictors were derived from Forest Inventory and Analysis observations and ancillary data on managerially uncontrollable factors—fire history, climate, weather, and topography—within California's massive 2021 Dixie fire. Logistic regression models were fitted to evaluate the effects of these predictors, with remotely sensed burn severity as the response. Using multiple model selection strategies to choose from among parsimonious predictor subsets that we structured to control for collinearity, high burn severity was consistently predicted (area under the receiver operating curve = 0.72–0.73) from just six variables: three stand characteristics—basal area of standing dead trees, basal area of mid-size or all live trees, and ladder fuel abundance—and three uncontrollable predictors—30-year mean maximum annual temperature and maximum wind gust speed and precipitation for the hour at which fire arrived at the stand. To demonstrate how these models might inform landscape treatment priority, we applied the models to publicly available, imputed rasters of the stand characteristics and to the uncontrollable factors listed above, evaluating map accuracy against Relative differenced Normalized Burn Ratio derived severity. Disappointing accuracy of the resultant maps might be improved as forest attribute imputation products begin to incorporate fine scale (e.g., Light Detection and Ranging) information capable of representing ladder fuels and as pixel scale models of weather at time of fire arrival become available.

Key words: Dixie fire, FIA plots, RdNBR-derived burn severity, imputation rasters, wind gust speed, ladder fuel

Introduction

Among the many relevant ecological and social drivers influencing forests globally, large wildfires containing large patches of high burn severity play an increasingly important role as their frequency increases (McLauchlan et al. 2020; Tyukavina et al. 2022). California's massive 2021 Dixie fire, the subject of the analysis reported here, provides one example of how such fires can transform vast forest areas over days to weeks with profound effects on habitat, biodiversity, and human lives. The increased frequency of high burn severity being delivered by climate change and other factors (Williams et al. 2019; Turco et al. 2023) has made developing comprehensive strategies to mitigate high-severity, stand-replacing fire a top priority [e.g., Wildfire Crisis Strategy by United States Department of Agriculture (USDA Forest Service 2023)]. A successful strategy requires a better understanding of the precursors to stand-replacing fire—especially where forests may be amenable to silvicultural treatments that can reduce the likelihood of high burn severity outcomes (Halpern and Antos 2022).

Managers have come to rely on routinely produced, spatially comprehensive representations of burn severity when planning post-fire response, thanks to the widespread availability of multi-spectral remotely sensed imagery with steadily improving spatial and temporal resolution (Robichaud et al. 2009; Miller et al. 2015; Background, Products & Applications | BAER 2025). They would also benefit from proactively generated maps of forest landscapes that identify where combinations of vegetation structure, climate, and topography that lead to high burn severity can be changed via fuels management to instead produce low burn severity outcomes—at least under the more moderate weather conditions that prevail for most days of most fires. Following Eidenshink et al. (2007), we define "burn severity" as the site-level, relative, fire-induced change with respect to live and dead vegetation and forest floor and evidence of such fire byproducts as ash and charcoal. As a relative metric, burn severity is inextricably linked to pre-fire condition. Burn severity indices constructed from remotely sensed data include (1) differenced Normalized Differenced Vegetation Index (dNDVI) (Hudak et al. 2007), which targets fire-induced change in the vigor of photosynthesizing vegetation; (2) Normalized Burn Ratio (NBR), calculated as the normalized difference of near- and shortwave-infrared reflectance (Key and Benson 1999); and (3) differenced Normalized Burn Ratio (dNBR), the difference in NBR between pre- and post-fire (Key and Benson 2006). Miller and Thode (2007) proposed a relativized version of dNBR, the Relativized differenced Normalized Burn Ratio (RdNBR) that makes burn severity measurements more commensurate across heterogenous vegetation types and levels of pre-fire biomass.

Given that distinguishing between stand-replacing fire and the absence thereof is essential for assessing the fire vulnerability or resilience of a forested landscape, it is important to select a burn severity metric closely related to change in live biomass. Studies evaluating these indices against field or drone-based measurements of canopy cover change and basal area mortality present a mixed picture but generally indicate that dNBR and RdNBR tend to outperform dNDVI (Escuin et al. 2008; Furniss et al. 2020). Without definitive evidence for the superiority of either dNBR or RdNBR at detecting stand-replacing fire, we selected the relativized index to account for variations across the heterogenous forest types found in the area burned by the Dixie fire (Miller and Thode 2007).

Burn severity is closely tied to fire behavior, which, in turn, depends on weather, topography, and fuels, arguably in that hierarchical/contingent order. Other than investing greater effort in reducing ignition probability during times of extreme weather, management can only hope to modify the last of these, fuels, via vegetation management. A capacity to generate spatially explicit predictions of burn severity from forest structure, contingent also on the other drivers, can potentially guide investment in fuels modification. Relating burn severity to forest structure, however, requires field measurements that coincide with burn severity assessments. The USDA Forest Service Forest Inventory and Analysis (FIA) program collects, compiles, analyzes, and publishes richly attributed and systematically quality-assured ground data on live forest vegetation and standing and down dead wood using consistent monitoring protocols from hundreds of thousands of forest inventory plots on a systematic grid sample (Bechtold and Patterson 2005; Gray et al. 2012). These data have proved fruitful fodder for numerous studies, including some that addressed forest fuels and fire hazard (Tinkham et al. 2018). Many fires encounter FIA plots every year (Eskelson et al. 2016), generating fire effects that can be related to the abundant data associated with each plot. Relevant FIA-derived data products include observations recorded during visits to these plots before fire arrived (Azuma 2004; Shaw et al. 2017), modeled predictions from that pre-fire data (e.g., Barker et al. 2019), delayed mortality (Barker et al. 2022), post-fire fuel dynamics (Eskelson and Monleon 2018), changes in carbon mass (Woo et al. 2021), and representations of burn severity based on remote sensing (Pelletier et al. 2021; Busby et al. 2023). A unique feature of fire effects analysis conducted using FIA plot data is that vegetation types and fire severities are represented in FIA data in proportion to their landscape occurrence, comprising an unbiased sample of all forests within fire footprints. Apropos to this study, which characterizes burn severity via remote sensing classification, data collected from pre-fire visits to these plots can also provide an accurate and highly detailed representation of the forest that a fire encountered. This offers rich opportunities for retrospective analysis of "natural experiments" when evaluated in light of fire outcomes at those locations, opening the possibility of predicting burn severity from forest attributes analogous to those contained in the FIA data.

As heat and aridity have increased with climate change, several California wildfires over the past few years were dominated by high-intensity fire behavior and set records as the largest fires in the recorded history of the US (Varga et al. 2022; https://www.fire.ca.gov). The Dixie fire ignited when a tree contacted an electrical distribution line on 13 July 2021. It burned 963 309 acres (3898 km^2) despite 104 days of intensive and expensive suppression effort (https://www.fire.ca.gov/incidents/2021/7/13/dixie-fire/) owing to vegetation fuels that had experienced an extended period of heat and drought. This extremely large fire offers a rare opportunity to analyze fire effects across a very broad range of pre-fire forest conditions and fire weather. An understanding of how stand structure relates to burn severity could prove invaluable to forest managers prospecting for stands that can benefit from management that enhances fire-resistance.

Before the advent of suppression, fire return intervals of 8–22 years were typical in the region where the Dixie fire burned (Moody et al. 2006). A century of fire suppression has elevated stand density and surface fuel accumulations, contributing to an increased incidence of large wildfires (Beaty and Taylor 2008; Lydersen et al. 2014). Some notable examples within what would become the Dixie fire footprint include the 2000 Storrie Fire, the 2007 Moonlight Fire, the 2008 Butte Lightning Complex, the 2008 Rich Fire, the 2010 Bar Fire, the 2012 Chips Fire, and the 2012 Reading Fire (https://gis.data.ca.gov/datasets/CALFIRE-Forestry::california-fire-perimeters-all-1/explore).

A preliminary Rapid Assessment of Vegetation Condition after Wildfire (RAVG) report and our personal observations during field visits on 22 September and 5 October 2021, indicate considerable variation in burn severity within the Dixie fire. One published analysis of this fire explored the effects of past fires on reburn severity (Taylor et al. 2022). Other drivers, including forest structure, surface fuel loading, land management objectives and associated silviculture practices, topography, long-term climate, and local weather on fire arrival may be at least as important. Local weather is so important that it must be accounted for, in some fashion, for the signal of other drivers to be discernable (Bessie and Johnson 1995).

Recent years have seen efforts to restore forests via mechanical fuel treatments (typically thinning) and prescribed fire. This strategy centers on rearranging and/or reducing woody fuels to offset the threats resulting from increasing wildfire incidence, drought, and a warming climate (Keeley et al. 2021). For nearly two decades, there have been calls to increase the pace and scale of forest treatments to promote resilience, particularly in the xeric forests of the western US that have experienced increasingly frequent and severe drought and large wildfires (e.g., North et al. 2021). A large, nationally coordinated, strategic response was unveiled in 2022 as the Wildfire Crisis Strategy (US Forest Service 2022*a*, 2022*b*; USDA Forest Service 2023). Given that it is not feasible to immediately apply fire resistance treatments in all forests, identifying forests most likely to burn as stand-replacing, ceteris paribus with respect to weather, etc., would be a substantial contribution that could help managers prioritize treatments for maximum benefit. Such predictions could also aid policy makers designing programs to encourage actions that enhance fire resistance.

Developing information and tools useful to forest managers needing to mitigate against high severity fire outcomes requires understanding the relationship between high burn severity and potential factors that might lead to that outcome. With a few dozen potential predictors derived from pre-fire forest structure observations on 187 FIA plots, model-derived weather and climate attributes, and static topographic site characteristics, we fit multi-variable logistic regression models to predict a binary burn severity classification (high severity, stand-replacing vs. not) derived from remotely sensed RdNBR data to learn which predictors are influential. Models were ranked by corrected Akaike information criterion (AICc), and a multi-model average was calculated following the methods in Anderson and Burnham (2004). The model selection process yielded insights into the relative importance of the candidate predictors that informed three parsimonious models predicting high-severity status at the FIA plot locations. Integrating these with a publicly available, spatially comprehensive imputation of FIA observations, we developed and evaluated an easily applied workflow to predict the probability of high burn severity over a forest landscape, contingent on imputed stand conditions and fire weather.

Methods

Study area

The Dixie fire burned through large swaths of the Sierra Nevada's Plumas National Forest, Lassen National Forest (situated on a transition zone between the Sierra Nevada and the Cascade Range), and much of Lassen Volcanic National Park (Fig. 1). It also extended north into the juniper-sagebrush steppes of the Modoc Plateau. Elevation ranges from 152 m in Feather River Canyon to 3187 m at the summit of Mount Lassen (US Geological Survey, MTBS 2017).

The Mediterranean climate here features cold, wet winters, and warm, dry summers. Owing to past management and disturbance, forest stands are heterogeneous within each forest type, including even- and uneven-aged true fir (white fir (*Abies concolor*) and red fir (*Abies magnifica*)) and/or lodgepole pine (*Pinus contorta*) at high elevation. Mixed conifer, coast Douglas-fir (*Pseudotsuga menziesii var. menziesii*), ponderosa pine (*Pinus ponderosa*), Jeffrey pine (*Pinus jeffreyi*), sugar pine (*Pinus lambertiana*), incense cedar (*Calocedrus decurrens*), white fir, and California black oak (*Quercus kelloggii*) types dominate the middle elevations, with a significant complement of stands planted to pure ponderosa pine. Foothill pine (*Pinus sabiniana*) and blue oak (*Quercus douglasii*) woodlands are most common at lower elevations. Hardwoods, such as aspen (*Populus tremuloides*) and willow (*Salix* spp.), are common in riparian zones and, at high elevations, abut meadows and lakes (Eyre 1980; Barbour and Major 1988).

Data sources and variables

Burn severity

We calculated the Relative differenced Normalized Burn Ratio (RdNBR) for all pixels within the final, mapped fire perimeter using Sentinel-2 imagery to represent burn severity. Sentinel-2's relatively fine-grained spatial and temporal resolutions (20 m pixels in the bands needed to calculate RdNBR and a 5-day return window; European Space Agency (ESA) 2015) offer substantial improvement over the Landsat Thematic Mapper (TM) and Enhanced Thematic Mapper Plus (ETM +) platforms' (30 m pixels and 16-day return window; Parks et al. 2014) typically used to obtain RdNBR.

RdNBR captures relative burn severity, making it ideal for comparing fire effects across a large and heterogenous landscape (Miller and Thode 2007; Figs. 2 and 3). Miller et al. (2009) reported that RdNBR-based models trained on multiple fires performed acceptably when predicting Composite Burn Index (CBI) of fires outside the training dataset. Widely deployed classified burn severity products [e.g., BAER (Background, Products and Applications | BAER 2025), RAVG (Background, Products & Applications | RAVG 2016), and Monitoring Trends in Burn Severity (MTBS, Eidenshink et al. 2007)] also rely on RdNBR, albeit derived from the less spatially resolved Landsat data, making findings from this study directly applicable for those relying on such products.

We composited the least cloudy Sentinel-2 pixels for the 2 weeks before the start of the Dixie fire (1–14 July 2021) and the same dates 1 year later (1–14 July 2022) in Google Earth Engine (Gorelick et al. 2017). For each composite, we calculated NBR as the normalized difference of the near infrared (Band 8) and the shortwave infrared band (Band 12):

$$\mathrm{NBR} = (\mathrm{Band}\,8 - \mathrm{Band}\,12)\,/\,(\mathrm{Band}\,8 + \mathrm{Band}\,12)$$

Following Miller and Thode (2007), we calculated RdNBR:

$$\mathrm{RdNBR} = \frac{(\mathrm{PreFireNBR} - \mathrm{PostFireNBR})}{\sqrt{\left|\frac{\mathrm{PreFireNBR}}{1000}\right|}}$$

A weighted average of the Sentinel-2 pixels overlapping each FIA macroplot was constructed with weights derived from the proportion of the macroplot area covered by each pixel (Pelletier et al. 2021). The four macroplot values per plot thus obtained were averaged to derive a mean RdNBR value for each plot. Negative RdNBR values indicate an increase in vegetation cover (Miller et al. 2009). Because we used RdNBR solely as a proxy for fire effects, plots with a negative mean RdNBR were reclassified to zero (i.e., unaffected by fire). Following the RdNBR threshold for severe fire pro-

Fig. 1. The analysis area is defined as the intersection of the 3898 km^2 Dixie fire perimeter (shown in red) and federal lands, comprised of the Lassen & Plumas National Forests and Lassen Volcanic National Park (green outline). The figure was created using QGIS version 3.44.1 and assembled from the following data sources: Dixie fire boundary (CALFIRE https://gis.data.ca.gov/datasets/CALFIRE-Forestry::california-fire-perimeters-all-1/explore), Lassen and Plumas National Forest boundaries (USDA Forest Service https://data.fs.usda.gov/geodata/edw/datasets.php?dsetCategory=boundaries). Base map from Bing Aerial Imagery, courtesy of Microsoft, and inset base map from OpenStreetMap, courtesy of the OpenStreetMap foundation.

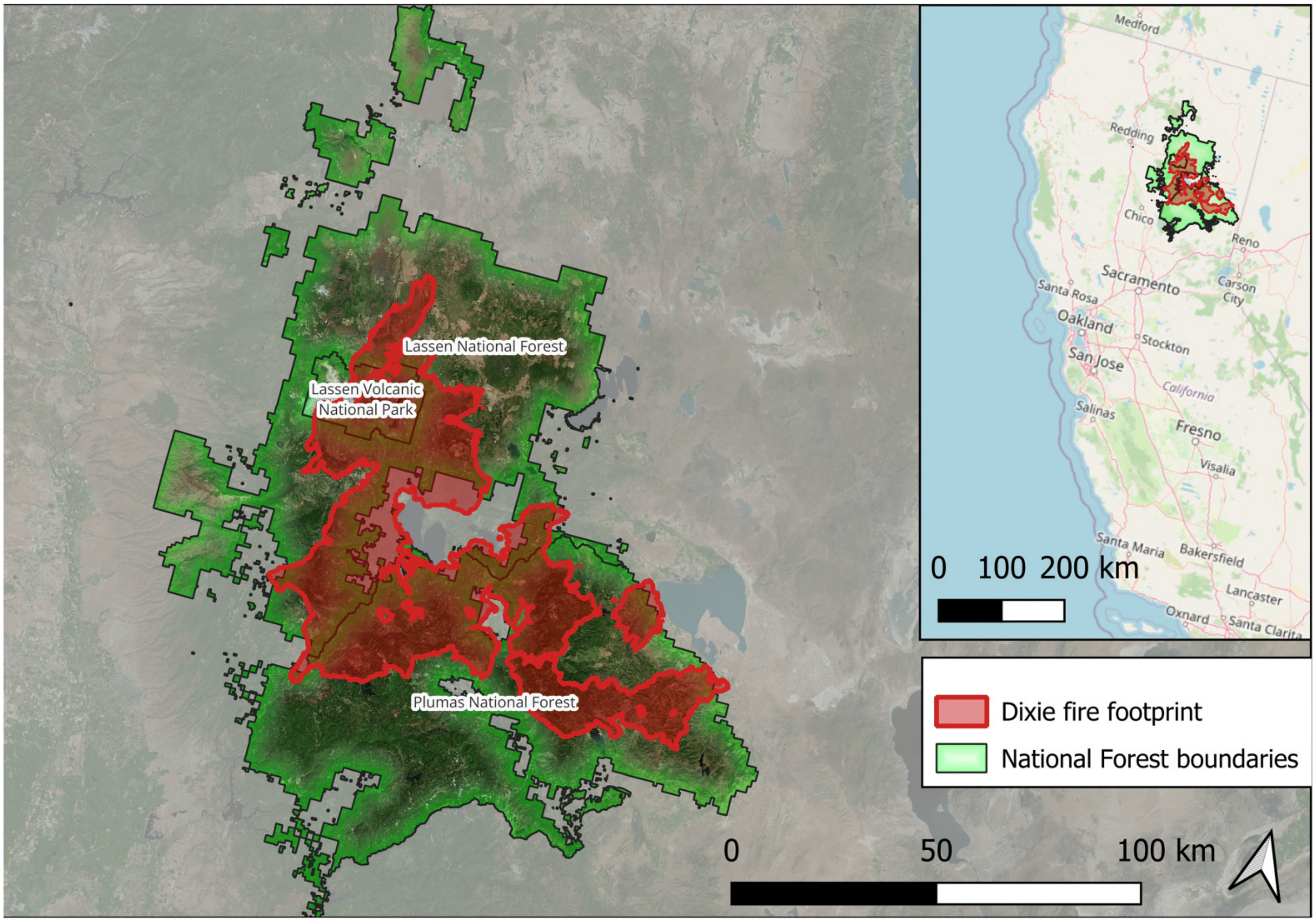

posed by Miller et al. (2009), we assigned a binary severity variable to each plot, coding plots with mean RdNBR > 574 as 1 (labeled "severe" and representing high burn severity, stand-replacing) and all others as 0 (labeled "not severe" and representing low-to-moderate severity).

Forest Inventory and Analysis plots

We derived all observations of pre-fire forest conditions from permanent inventory and monitoring plots in the nationally consistent, continuous FIA system, for which protocols are defined and documented in both database documentation [Forest Inventory and Analysis Database (FIADB) Users Guide; Burrill et al. 2021] and regional field guides (USDA Forest Service PNW Research Station FIA 2022c). These data included plots collected on both FIA's standard intensity (3.11 mi. (5 km)) sample grid and from spatially intensified grids installed by the Forest Service Region 5 using the same protocol and data compilation system. The plot "footprint" is a mapped design consisting of a sampled area formed by a quartet of 24 ft (7.3 m) radius subplots for sampling trees larger than 5 in. (12.7 cm) diameter at breast height (DBH, measured at 4.5 ft (1.37 m) above the ground). Co-located with each subplot is a 6.8 ft (2.1 m) radius microplot to sample small trees and a 58.9 ft (18 m) radius macroplot on which the largest trees (>24 in. (61.0 cm) in diameter) are sampled. The quartet is arranged as three satellite subplots arrayed symmetrically around a central subplot at 120 ft (36.6 m) distance and 120-degree intervals. This sampled area is partitioned into separate "conditions" when delineation-qualifying differences (e.g., in owner group, forested status, reserve status, forest type, stand size class, tree density class) exist and minimum condition size and shape criteria are satisfied. Site attributes such as slope, site quality, stand age, forest type, and landowner group are defined and collected at the condition level. All trees on each forested condition are assessed for status (live or dead), measured for diameter, and assessed for crown ratio, defect and disease, with a subsample assessed

 Can. J. For. Res. 55: 1–20 (2025) | dx.doi.org/10.1139/cjfr-2024-0305

Fig. 2. Fire severity varied within the Dixie fire final perimeter, as shown here for facets of the forest landscape in the vicinity of Mt. Lassen (indicated as a reference point by the orange arrow): (A) From the south and relatively close-by, (B) from the north and relatively close-by, with multiple legacy fire scars identifiable, (C) from the south and far-away with burned young plantation in the foreground, and (D) from the south at great distance with clear depiction of variation in burn severity. Photo credit: Jianwei Zhang.

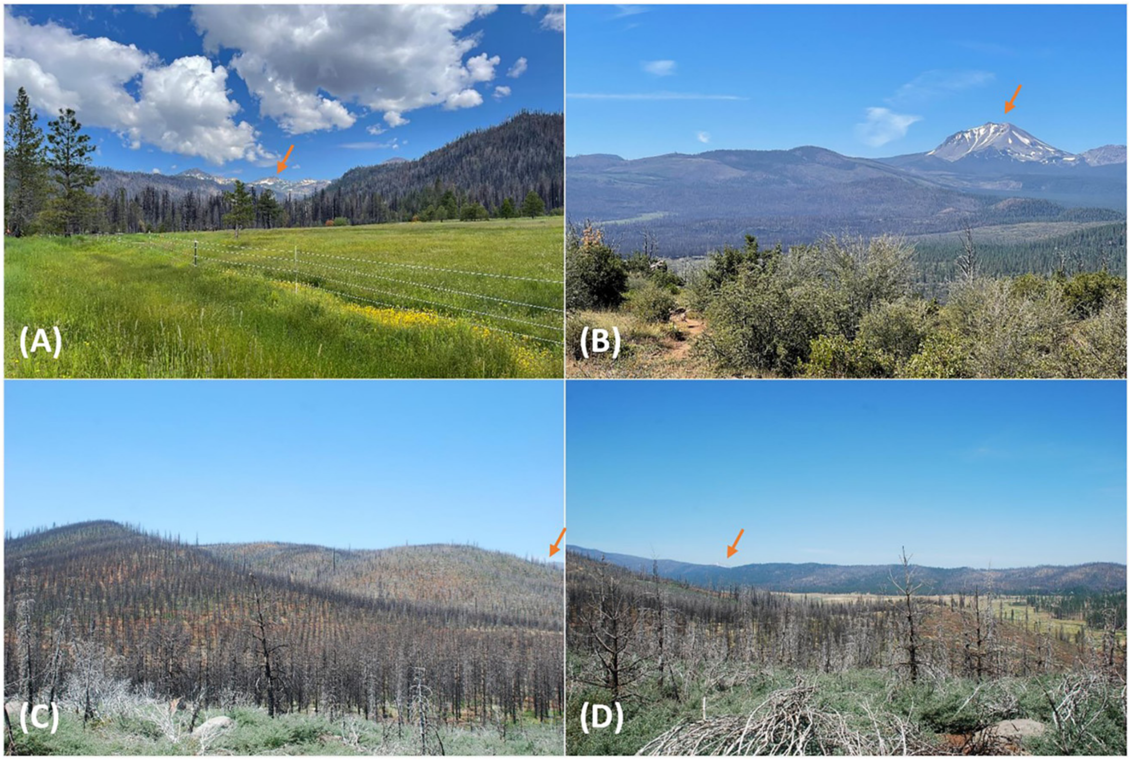

for height to provide a basis for imputing heights of those not assessed.

We analyzed data from the most recent pre-fire visit to each of the 275 plots sited within the final Dixie fire footprint on public land (i.e., excluding private land), ensuring an accurate pre-fire representation of forest attributes by filtering out plots:

- Sixty one plots were eliminated for falling within CalFire historical fire perimeters (https://gis.data.ca.gov/datasets/CALFIRE-Forestry::california-fire-perimeters-all-1/explore) with years between the plot visit (PLOT.MEASYR) and 2021, leaving 214 plots.
- Three plots were eliminated because nonforest conditions comprised >50% of the plot area, leaving 211 plots.
- Twenty four plots were eliminated because, while classified as forest land, no live trees were recorded at the most recent pre-fire visit, leaving 187 plots.

This subset yielded 187 forested FIA plots, inventoried between 2003 and 2019, with a median inventory year of 2016, containing 6941 measured trees (after data cleaning) of 18 species. Seventy one percent of the selected plots were inventoried ≤5 years before the Dixie fire in 2021, providing a relatively recent sample of pre-fire conditions. Burn severity on 109 plots (58%) was classed as “Severe”, and on 78 plots (42%) was classed as “Not Severe” (Fig. 3).

Variable overview

Thirty-five predictor variables were developed from the inventory data and other sources to represent stand structure, fire history, climate, weather, and topography (Table 1). To represent pre-fire stand structure, we calculated 15 variables from the FIA database. Due to high collinearity among them, each stand structure variable was assigned to one of three sub-groups: lateral canopy fuel continuity (referred to as “horizontal” stand structure measurements), ladder fuels (“vertical” stand structure), or “unrestricted” (neither horizontal nor vertical). Horizontal stand structure included basal area per acre (BAPA) (overall and stratified by diameter), trees per acre (TPA) (overall and stratified by diameter), and canopy bulk density. Vertical stand structure included number of canopy strata, canopy base height, and proportion of canopy cover in trees for which crown base is less than either 7 ft (2.1 m) or 20 ft (6.1 m). The unrestricted variables included percentage of basal area in fire-resistant species, percentage of basal area in hardwoods, and BAPA of standing dead trees. We also collected fire history data for each plot (years since the most recent fire and severity of that fire), but did not include this in the final candidate variable list due to the preponder-

Fig. 3. Map of Sentinel-2 derived Relative differenced Normalized Burn Ratio (RdNBR) at 20 m cell resolution for the Dixie footprint, classified into severe and not-severe using the RdNBR > 574 cutoff proposed in Miller et al. (2009). The location of Mt. Lassen is marked with an orange arrow to contextualize the images in Fig. 2. The approximate locations of the 187 Forest Inventory and Analysis (FIA) plots used are overlaid (black circles). The FIA locations depicted here are the publicly available coordinates fuzzed to within ~0.71 miles (1.14 km) of the true plot location to comply with the Food Security Act of 1985 (H.R. 2100). Gaps in the plot coverage over the fire footprint are typically either privately owned or non-forest. The figure was created using QGIS version 3.44.1 and assembled from the following data sources: Dixie fire boundary (CALFIRE https://gis.data.ca.gov/datasets/CALFIRE-Forestry::california-fire-perimeters-all-1/explore), Sentinel-2 derived burn severity (European Space Agency), FIA fuzzed plot locations (USDA Forest Service). Base map from 3D Elevation Program, courtesy of US Geological Survey.

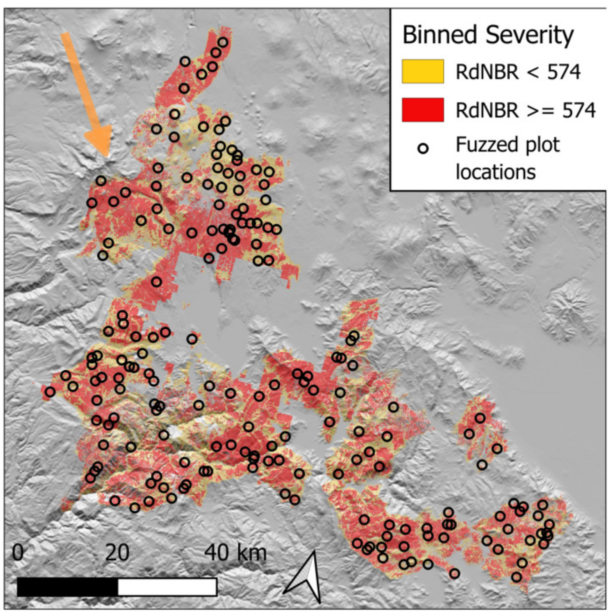

ance of fire-excluded plots. To account for possible climate-related drivers of burn severity, we associated 30-year climate normals with each plot (maximum annual temperature, maximum annual vapor pressure deficit, mean annual precipitation). We also estimated weather on the day and hour of fire arrival (daily maximum temperature, daily precipitation, daily mean wind speed, hourly precipitation, hourly mean wind speed, hourly air temperature, hourly fuel temperature, hourly relative humidity, hourly vapor pressure deficit, and hourly maximum wind gust speed). To represent topography, we calculated elevation, slope, aspect, and a terrain ruggedness index (TRI) for each plot. Eleven variables were eliminated due to correlation or an inadequate number of non-null cases, leaving 24 candidate variables to be included in model selection.

Stand structure (horizontal)

Stand-level live TPA was calculated by summing the TPA (TPA_UNADJ), defined as inverse of the tree-size specific plot size on which trees were sampled, for all live tree records in the condition. On plots with multiple conditions, the TPA_UNADJ value for each tree was scaled by the condition proportion associated with the tree's diameter. Smaller trees are sampled only at the sub- or micro-plot level, and these differences in sampling area must be accounted for when developing density estimates (FIADB Users Guide; Burrill et al. 2021). To account for the effect of tree size on fire resistance, stratified versions of TPA were calculated for 0 in. < DBH ≤ 10 in. (0–25.4 cm), 10 in. < DBH ≤ 21 in. (25.4–53.3 cm), and DBH > 21 in. (53+ cm) (abbreviated as *TPA_leq10*, *TPA_10_21*, and *TPA_gt21*, respectively).

Live BAPA was calculated identically to TPA with the added step of multiplying the TPA_UNADJ property by the tree's basal area, calculated as $\left(\frac{\mathrm{DBH}}{2}\right)^2 \cdot \pi$. Analogous to TPA, we calculated stratified versions for DBH classes of 0–10 in. (0–25.4 cm), 10–21 in. (25.4–53.3 cm), and 21+ in. (53+ cm) (abbreviated as *BAPA_leq10*, *BAPA_10_21*, and *BAPA_gt21*, respectively).

Canopy bulk density (*Canopy_density*, Cruz et al. 2003) was calculated using the fire and fuels extension of the forest vegetation simulator (FFE-FVS) (Reinhardt 2003). A plot-level weighted average was calculated for plots with multiple conditions by using condition proportion (CONDPROP_UNADJ in the FIA database) as the weight.

Stand structure (vertical)

The FFE-FVS (Reinhardt 2003) was used to calculate canopy base height (*Canopy_Ht*, Cruz et al. 2003) and the number of canopy strata for each forested condition (abbreviated as *Number_of_strata* and derived from attributes in the POTFIRE and STRCLASS table outputs of that model). Plot level values for these attributes were obtained as weighted averages with condition proportion (CONDPROP_UNADJ in the FIA database) as the weight.

We also calculated the percentage of tree crown area per acre belonging to trees with a crown height less than or equal to 7 ft (2.13 m) and the same variable for trees with crown height less than or equal to 20 ft (6.10 m) (abbreviated as *Ladder_frac_7* and *Ladder_frac_20*, respectively). Crown area per acre represented by each tree was calculated from measured DBH, tree height, and the TPA adjustment factor using the equations for crown diameter specified for the Inland California and Southern Cascades (CA) variant of FVS (Dixon 2002; Keyser 2008).

Stand structure (unrestricted)

To account for the variability in fire resistance among tree species, we drew on results from the First Order Fire Effects Model (Peterson 2007) to classify individual trees as resistant based on the DBH threshold past which mortality for trees of that species drops below 30%. Red fir (*Abies magnifica*) and ponderosa pine (*Pinus ponderosa*) were classed as resistant for

 Can. J. For. Res. **55:** 1–20 (2025) | dx.doi.org/10.1139/cjfr-2024-0305

Table 1. Sources and category of all variables evaluated in this study.

Variable	Abbreviation	Units	Source	Status
Response				
RdNBR	weighted_mean_RdNBR_macro	Unitless indicator variable	Sentinel-2	
Binary severity (RdNBR ≥ 574)	Severe	Unitless indicator variable	Sentinel-2	
Independent (forest stand condition)				
Basal area per acre	BAPA	ft^2 ac^{-1}	FIA	
Basal area per acre for trees with DBH ≤ 10	BAPA_leq10	ft^2 ac^{-1}	FIA	
Basal area per acre for trees with 10 < DBH ≤ 21	BAPA_10_21	ft^2 ac^{-1}	FIA	
Basal area per acre for trees with DBH > 21	BAPA_21	ft^2 ac^{-1}	FIA	Removed due to high correlation
Trees per acre	TPA	trees ac^{-1}	FIA	Removed due to high correlation
Trees per acre for trees with DBH ≤ 10	TPA_leq10	trees ac^{-1}	FIA	
Trees per acre for trees with 10 < DBH ≤ 21	TPA_10_21	trees ac^{-1}	FIA	Removed due to high correlation
Trees per acre for trees with DBH > 21	TPA_gt21	trees ac^{-1}	FIA	
Percentage of basal area belonging to resistant species	Res_pct_ba	%	FIA, FOFEM	
Basal area belonging to standing dead trees	Standing_dead_pct_ba	ft^2 ac^{-1}	FIA	
Percentage of basal area (BA) belonging to hardwoods	Hard_pct_ba	%	FIA	
Years since last fire	Years_since_burn	Years	Fire and Resource Assessment Program (FRAP)	Removed due to null observations
Severity of last fire	Prev_burn_sever	Unitless	MTBS	Removed due to null observations
Number of canopy strata	Number_of_strata	Unitless	FIA, FVS	
Canopy base height	Canopy_Ht	Ft	FIA, FVS	
Canopy bulk density	Canopy_Density	kg m^{-3}	FIA, FVS	
Proportion of canopy area per acre < 20 ft	Ladder_20_Frac	%	FIA, FVS	
Proportion of canopy area per acre < 7 ft	Ladder_7_Frac	%	FIA, FVS	
Independent (climate)				
30-year average maximum annual temperature	Tmax_30_yr	Degrees C	Parameter-elevation Regressions on Independent Slopes Model (PRISM)	
30-year average maximum vapor pressure deficit	Vpd_max_30_yr	hPa	PRISM	Removed due to high correlation
30-year average precipitation	Precip_30_yr	in.	PRISM	
Independent (weather)				
Daily maximum temperature	Daily_tmmx	K	GRIDMET	
Daily minimum relative humidity	Daily_min_relh	%	GRIDMET	
Daily precipitation	Daily_precip	mm	GRIDMET	Removed due to null observations
Daily wind speed	Daily_windspd	m s^{-1}	GRIDMET	
Hourly precipitation*	Hr_precip	mm	RAWS	
Hourly wind speed*	Hr_windspd	m s^{-1}	RAWS	Removed due to high correlation
Hourly air temperature*	Hr_airtemp	Degrees C	RAWS	Removed due to high correlation
Hourly fuel temperature*	Hr_fueltemp	Degrees C	RAWS	
Hourly relative humidity*	Hr_relh	%	RAWS	
Hourly vapor pressure deficit*	Hr_vpd	hPa	RAWS	Removed due to high correlation
Hourly maximum wind gust speed*	Hr_spd_maxgust	m s^{-1}	RAWS	
Binned hourly maximum wind gust speed (>8.5 m s^{-1})	High_wind	Indicator	RAWS	
Independent (topographic)				
Elevation	ELEV	Ft	FIA	Removed due to high correlation

Table 1. (*concluded*).

Variable	Abbreviation	Units	Source	Status
Terrain roughness	Terrain_rough_idx	m	3DEP	Removed due to high correlation
Aspect (Beers-transformed)	Beers_aspect	Unitless	FIA	
Slope	Slope	%	FIA	

Note: Sentinel-2—a European wide-swath, high-resolution, multi-spectral imaging mission; FIA—the Forest Inventory and Analysis (FIA) program of the U.S.; FOFEM—a First Order Fire Effects Model; FVS—forest vegetation simulator; GRIDMET—the Gridded Surface Meteorological dataset; RAWS—the Remote Automatic Weather Stations system; 3DEP—the United States Geographic Survey 3D Elevation Program. Units are those in which these data are provided. Status accounts for variables ultimately not included in the models developed. RdNBR, Relative differenced Normalized Burn Ratio; DBH, diameter at breast height; TPA, trees per acre; BAPA, basal area per acre.

trees with DBH > 15 in. (38.1 cm), and white fir (*Abies concolor*), incense cedar (*Calocedrus decurrens*), jeffrey pine (*Pinus jeffryi*), and douglas-fir (*Pseudotsuga menziesii*) were classed as resistant when DBH exceeded 20 in. (50.8 cm) in diameter. After classifying each tree as either resistant or not, we calculated the percentage of live BAPA on each plot composed of resistant trees (abbreviated as *Res_pct_ba*).

We calculated the BAPA composed of standing dead trees (abbreviated *Standing_dead_ba*). Such trees have a value of 1 for the STANDING_DEAD_CD attribute in the FIA database. We also quantified the percentage of live BAPA in hardwood species (abbreviated as *Hard_pct_ba*). Of the 17 species found on plots in the Dixie fire, six were hardwoods: bigleaf maple (*Acer macrophyllum*), bitter cherry (*Prunus emarginata*), California black oak (*Quercus kelloggii*), canyon live oak (*Quercus chrysolepis*), pacific dogwood (*Cornus nuttallii*), and quaking aspen (*Populus tremuloides*).

Fire history

The legacy fire experience of each plot was considered as a candidate predictor, however, only 19 out of 187 plots had burned within the 15 years prior to the Dixie wildfire, and of those, the most recently burned had burned 9 years prior. Past 15 years, the effect of fuel depletion on fire severity in Northern California has been observed to diminish (Harris and Taylor 2017; Taylor et al. 2021). Due to the large number of null observations, time since fire and prior burn severity were not included in the set of candidate predictors.

Climate

Representation of long-term climate was drawn from PRISM 30-year normal rasters with a spatial resolution of 800 m (PRISM Climate Group 2014). Raster cells were extracted at plot centers to assign three 30-year average climate variables to each plot: maximum annual temperature, maximum vapor pressure deficit, and average annual precipitation (abbreviated as *Tmax_30_yr*, *Vpd_max_30_yr*, and *Precip_30_yr*, respectively).

Weather and wind

To assign daily and sub-daily weather variables to each plot, we used the 2021 Visible Infrared Imaging Radiometer Suite (VIIRS) Suomi National Polar-orbiting Partnership (NPP) Active Fire product from the National Aeronautics and Space Administration (NASA) Fire Information for Resource Management System (EARTHDATA 2025). VIIRS active fire records are supplied as coordinates corresponding to pixel centers with a timestamp recording the time of the first overpass in which the thermal signature of a fire was detected. Although VIIRS has a spatial resolution of 1230 ft (375 m), within the Dixie fire footprint multiple overpasses resulted in VIIRS fire detection points with an average nearest neighbor distance of 420 ft (128 m). We generated a smoothed triangulated irregular network to interpolate between the time-stamped points, creating a 98 ft (30 m) raster time surface (Fig. 4).

Day and hour of fire arrival at each plot was estimated by overlaying exact plot locations on the fire progression raster described above. These "time stamps" provided the basis for sampling Gridded Surface Meteorological dataset (GRIDMET) daily weather rasters for estimates of daily maximum temperature, minimum relative humidity, and wind speed (abbreviated *Daily_tmmx*, *Daily_min_relh*, *Daily_windspd*) (Abatzoglu 2013), and for assigning hourly weather data from the nearest Remote Automated Weather Station (RAWS) to each plot (Fig. 5). Daily precipitation was considered but dropped from analysis because only six plots burned on days for which GRIDMET recorded nonzero precipitation. Because of uncertainty regarding the exact burn time, we tested several temporal windows for averaging seven RAWS weather variables (precipitation [*Hr_precip*], wind speed [*Hr_windspd*], air temperature [*Hr_airtemp*], fuel temperature [*Hr_fueltemp*], relative humidity [*Hr_relh*], max wind gust speed [*Hr_spd_maxgust*], vapor pressure deficit [*Hr_vpd*]) and found that a 7 h window centered on the estimated burn hour produced the greatest area under the receiver operating curve (AUC) when tested in a naïve model consisting of basal area, 30-year maximum temperature, canopy base height, hourly air temperature, and hourly windspeed.

Topography

We calculated per-plot mean of the slope, elevation, and aspect values provided for each subplot in the FIA database (abbreviated *Slope*, *ELEV*, and *Beers_aspect*, respectively). We transformed the aspect variable to be noncyclic with the formula in Beers (1966). We derived a TRI raster from one-third arcsecond 3D Elevation Program elevation data and sampled it at plot centers (abbreviated *Terrain_rough_idx*) (Stoker and Miller 2022).

Fig. 4. Estimated Dixie fire arrival time in Julian hours [hours since midnight Coordinated Universal Time (UTC), 1 January 2021]. Estimates were generated by using a triangulated irregular network to interpolate time-stamped fire detection pixel centers from the 2021 Visible Infrared Imaging Radiometer Suite (VIIRS) Suomi NPP Active Fire product. The figure was created using QGIS version 3.44.1 and assembled from the following data sources: Dixie fire boundary (CALFIRE https://gis.data.ca.gov/datasets/CALFIRE-Forestry::california-fire-perimeters-all-1/explore), VIIRS-derived burn time (NASA Fire Information for Resource Management System), base map from 3D Elevation Program, courtesy of US Geological Survey.

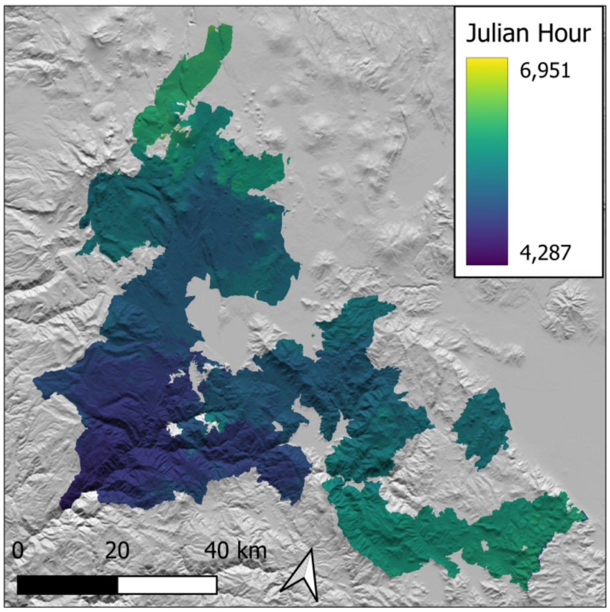

Fig. 5. Remote Automated Weather Stations (RAWS) and the portions of the fire to which weather data from those stations was used to represent hourly weather. The overlaid polygons (black lines) are Voronoi polygons that each enclose the set of geographic points closer to a given RAWS than any other RAWS. These polygons were used to link each Forest Inventory and Analysis plot to weather measurements at fire arrival time as observed by the closest station. The figure was created using QGIS version 3.44.1 and assembled from the following data sources: Dixie fire boundary (CALFIRE https://gis.data.ca.gov/datasets/CALFIRE-Forestry::california-fire-perimeters-all-1/explore), RAWS locations (National Weather Service). Base map from 3D Elevation Program, courtesy of US Geological Survey.

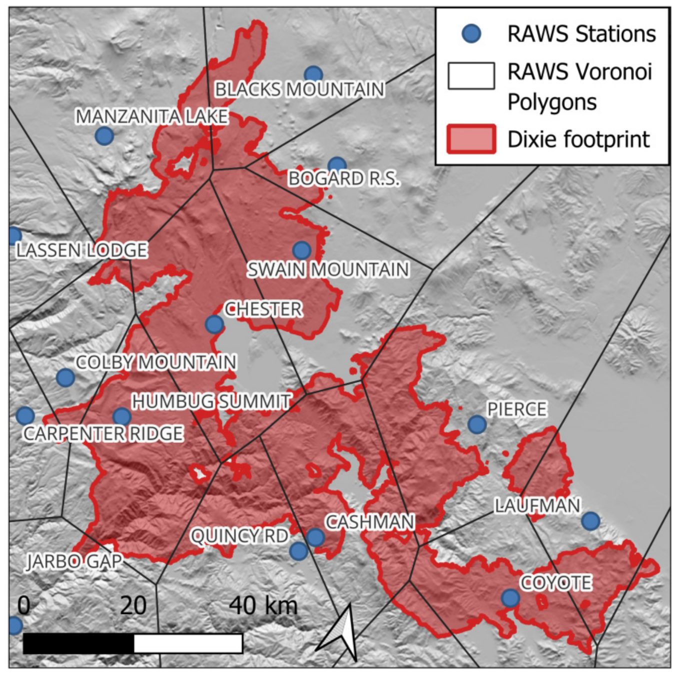

Model design and development

To assess the drivers of burn severity, we fit binomial regression models with a logit link to 24 of the 35 potential predictor variables spanning stand conditions (horizontal, vertical, and unrestricted), weather, climate, and topography with the binary severity code as the dependent variable (Table 1; Fig. 6). We used these logistic regression models to develop a multi-model average, following the methods in Anderson and Burnham (2004). To standardize the model coefficients and emphasize their relative importance, we scaled and centered each variable using the *scale* function in R prior to fitting the model (R Core Team 2023).

Variable elimination

To reduce the number of candidate models that would be tested, we conducted a preliminary correlation analysis to remove the most highly correlated candidate variables prior to testing models (Harrell 2001). Pearson's correlation coefficient was computed for every variable pair in the scaled and centered dataset to identify the most correlated pair of variables, eliminating the variable with the greater mean correlation with all other variables in the dataset. This process was iterated until no pairs of variables remained with a correlation coefficient greater than or equal to 0.85, a conservative threshold selected to limit the risk of discarding a strong predictor. This resulted in the elimination of TPA (0.994 correlation with TPA with diameter < 10 in. (25.4 cm)), TPA with diameter between 10 and 21 in. (25.5–53.3 cm) (0.972 correlation with basal area in the same diameter range), 30-year vapor pressure deficit and terrain elevation (correlation coefficients of −0.977 and −0.965 with 30-year maximum temperature, respectively), hourly windspeed (0.964 correlation with hourly maximum wind gust speed), TRI (0.945 correlation with terrain slope), hourly vapor pressure deficit (0.937 correlation with hourly air temperature), BAPA for trees greater than 21 in. (53.3 cm) diameter (0.925 correlation with TPA in the same diameter range), and hourly air temperature (0.895 correlation with hourly fuel temperature). Figure S1 shows the correlation structure of the 24 variables that remained after these eliminations.

Fig. 6. Box plots of every candidate variable for severe and not-severe plots with two-tailed *t*-test *p*-value for each (posted at the top of each panel). Differences between plots with severe and not-severe burn severity were significant ($\alpha = 0.05$) for elevation, hourly precipitation, hourly relative humidity, hourly maximum wind gust speed, hourly mean windspeed, 30-year vapor pressure deficit, and 30-year maximum temperature. DBH, diameter at breast height.

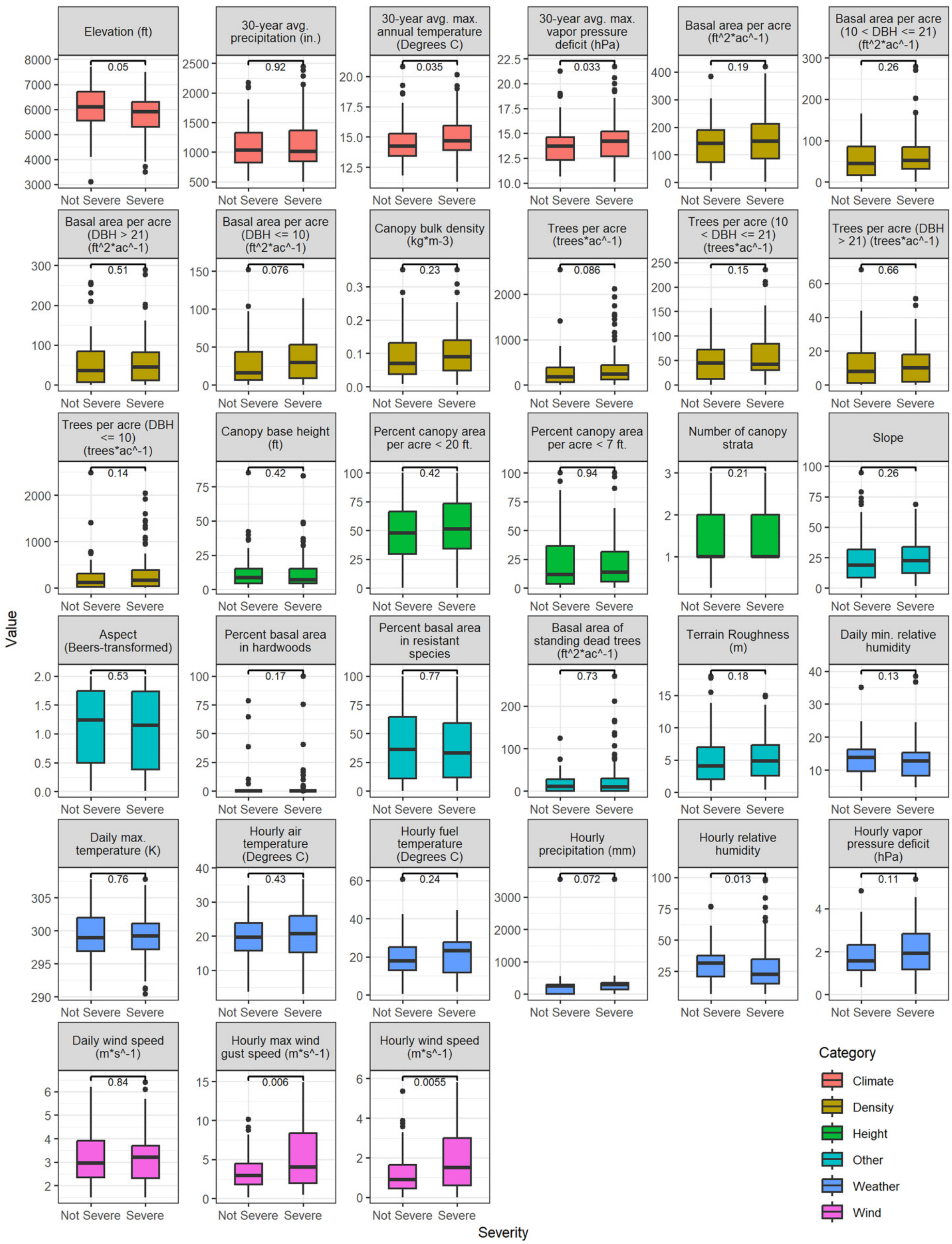

Can. J. For. Res. **55:** 1–20 (2025) | dx.doi.org/10.1139/cjfr-2024-0305

Considerations for model construction, selection, and evaluation

To identify parsimonious subsets of the remaining 24 variables, we used AICc to rank candidate models that met our criteria. To preempt the selection of correlated variables and ensure the representation of each class of predictor known to influence burn severity, variables were partitioned into correlated and thematically focused groups, and these groups were then used to restrict the set of tested models. Restricting the set of candidate models to those that comport with a prior understanding of burn severity drivers reduces the likelihood of landing on a spurious or overfitted model, a common pitfall of unrestricted model selection (Anderson and Burnham 2004).

Candidate models were limited to those with exactly one variable representing lateral canopy fuel continuity (horizontal stand structure: BAPA, TPA, or canopy bulk density), and one representing ladder fuel connectivity (vertical stand structure: percent of canopy cover on trees with crown base heights below 7 or 20 ft (2.1 or 6.1 m), number of canopy strata, or canopy base height). Wind speed was allotted a separate group from other short-term weather variables in light of its high importance and acceptably low correlation with other weather metrics (Fig. S1). Candidate models were allowed at most one variable representing wind speed (daily windspeed, hourly max wind gust speed, or binary wind gust speed class), at most one representing long-term climate (30-year precipitation, 30-year maximum temperature), and one representing short-term site temperature or aridity (daily minimum relative humidity, daily max temperature, hourly precipitation, hourly fuel temperature, or hourly air temperature). The remaining "unrestricted" stand structure and topography variables (Beers-transformed aspect, terrain slope, basal area of standing dead trees, percentage of live basal area comprised of resistant species, and percentage of live basal area comprised by hardwood species) were allowed to appear in any combination. Finally, models with more than 12 parameters were excluded to ensure a ratio of at least 15 observations per parameter (Harrell 2001). This approach to model construction ensured that no variable pairs within a candidate model would have a correlation coefficient greater than 0.66 (Fig. S1), limiting the impact of collinearity on coefficient estimates (Dormann et al. 2013).

Goodness of fit for all tested models was assessed by calculating cross-validated AUC (via the *ROCR* package for R; Sing et al. 2005) by randomly partitioning the data into five "folds", fitting the candidate model to four with the fifth reserved as test data, repeated across 10 random partitions. Reported AUC were averaged across all 50 tests.

Akaike weights were calculated for the set of models with ΔAICc < 7 (the upper bound of moderate evidence suggested by Anderson and Burnham (2004)) as:

$$w_i = \frac{\exp\left(-\frac{1}{2}\Delta_i\left(\text{AICc}\right)\right)}{\sum_{i=1}^{K}\exp\left(-\frac{1}{2}\Delta_i\left(\text{AICc}\right)\right)}$$

These were used to weight a multi-model average created via the *model.avg* function in the *MuMIn* R package (Bartoń 2025). This averaged model was evaluated by calculating AUC and, after binning predictions with a cutoff of 0.5, percent accuracy and Cohen's kappa. The kappa statistic compares agreement between raters and is calculated as

$$\kappa = \frac{2\times\ (\text{TP}\times\text{TN}-\text{FN}\times\text{FP})}{(\text{TP}+\text{FP})\times\ (\text{FP}+\text{TN})+(\text{TP}+\text{FN})\times\ (\text{FN}+\text{TN})}$$

where TP, TN, FN, and FP denote true positive, true negative, false negative, and false positive, respectively. A value of 1 indicates perfect agreement, whereas a value of 0 is consistent with the level of agreement expected from the null model, or random allocation. To detect possible spatial autocorrelation, a spatial correlogram was generated from plot coordinates and model residuals with the *correlog* function in the *ncf* R package (Bjornstad 2022).

Mapping

We used Landscape Ecology, Modeling, Mapping and Analysis (LEMMA) gradient nearest-neighbor imputations (Ohmann et al. 2011) to estimate stand condition variables for every 30 m pixel in Lassen and Plumas National Forests. Hourly weather estimates were assigned to each pixel in the Dixie fire footprint using the interpolated fire progression map by matching pixel centers with the nearest RAWS. Daily weather, climate, and topographic rasters were resampled to match the 30 m pixel resolution of the LEMMA rasters.

We selected three parsimonious models to test on imputed stand conditions. One consisted of the five variables with the largest coefficients in the multi-model average, and the other two were those with the highest AUC within the set of models with ΔAICc < 2. The averaged model was not used, as the large number of variables it incorporates limit its feasibility as the basis for a management tool. These models, as fitted to the FIA plots, were applied to each pixel within the Dixie footprint and the resulting predictions were evaluated using the same metrics (AUC, accuracy, and Cohen's kappa). Spatial autocorrelation was measured by calculating global Moran's I on the map of residuals. To test sensitivity to scale and address concerns about the granularity of LEMMA predictions, we also assessed accuracy after down-sampling the predictions by a factor of 27–65 ha pixels (approximately one quarter-section).

To demonstrate how these models might be applied to assess the risk of high burn severity across the landscape, the 5-parameter model selected based on model averaging was used to create maps of high burn severity likelihood covering the entirety of Lassen and Plumas National Forests by replacing the hourly wind map with uniform rasters of 50th, 90th, and 98th percentile hourly wind speed observations from RAWSs over the period that the Dixie fire burned.

To test whether it is plausible that the fit of the prediction maps is primarily driven by imputation error, we compared the 5-variable model's goodness of fit on sampled LEMMA data to its goodness of fit to a dataset with intentionally perturbed stand condition estimates. The former drew on a sample of 227 pixels aligned to a regular 1.86 mi (3 km) grid,

Table 2. Parameters for the multi-model average calculated from models with ΔAICc < 7.

Parameter	Category	β	2.5% Confidence Interval (CI)	97.5% CI	Subset β	Σw_i
Intercept		0.426	0.097	0.755	0.426	NA
tmax_30_yr	Climate	0.481	0.087	0.885	0.486	0.99
precip_30_yr	Climate	NA	NA	NA	NA	0
BAPA_10_21	Horizontal	0.181	− 0.016	0.818	0.401	0.45
BAPA	Horizontal	0.128	− 0.028	0.771	0.371	0.346
BAPA_leq10	Horizontal	0.013	− 0.177	0.529	0.176	0.072
Canopy_Density	Horizontal	0.005	− 0.236	0.472	0.118	0.044
TPA_leq10	Horizontal	0.005	− 0.237	0.467	0.115	0.043
TPA_gt21	Horizontal	0.005	− 0.311	0.550	0.119	0.046
Ladder_20_frac	Vertical	0.476	0.043	0.968	0.506	0.941
Number_of_Strata	Vertical	0.001	− 0.213	0.446	0.116	0.009
Ladder_7_frac	Vertical	0	− 0.282	0.362	0.04	0.003
Canopy_Ht	Vertical	− 0.011	− 0.610	0.144	− 0.233	0.046
standing_dead_ba	Other	0.469	0.054	0.929	0.491	0.955
res_pct_ba	Other	0.01	− 0.507	0.592	0.042	0.239
hard_pct_ba	Other	− 0.013	− 0.407	0.283	− 0.062	0.202
beers_aspect	Other	− 0.017	− 0.414	0.252	− 0.081	0.216
SLOPE	Other	− 0.049	− 0.550	0.208	− 0.171	0.289
hr_precip	Weather	0.034	− 0.125	0.511	0.193	0.173
hr_relh	Weather	0.025	− 0.198	0.608	0.205	0.124
daily_min_relh	Weather	− 0.013	− 0.466	0.195	− 0.136	0.096
daily_tmmx	Weather	− 0.018	− 0.577	0.230	− 0.173	0.103
hr_fueltemp	Weather	− 0.068	− 0.656	0.104	− 0.276	0.246
hr_spd_maxgust	Wind	0.755	0.296	1.214	0.755	1
daily_windspd	Wind	NA	NA	NA	NA	0

Note: Coefficients are based on scaled and centered variables, and represent the mean parameter value across all models, weighted by Akaike weight. The values in the Subset *β* column represent the parameter values averaged only across those models in which the parameter appears (i.e., nonzero). When this value is substantially larger than the corresponding full-average parameter estimate, the variable appears primarily in models with low Akaike weights and is likely of low importance. The Σw_i column lists the sum of Akaike weights for all models in which a variable appears and also indicates relative importance. AICc, corrected Akaike information criterion.

roughly approximating the spacing of FIA plots. Since these sampled pixels draw on the same wind and climate layers used to assign values to the FIA plots, they differ from the plots only in their estimation of stand conditions. The fuzzed dataset substituted 20 ft (6.1 m) crown percentage and snag basal area with random values drawn from a Gaussian distribution with the same mean and standard deviation. Basal area of mid-size trees was "jittered" by adding random values from a Gaussian distribution with the same mean and half the standard deviation.

Results

Top-ranked models' selection

Three hundred forty-nine models had a ΔAICc less than or equal to 7 (the top 116 models with ΔAICc ≤ 5 are presented in Table S2). Total BAPA and BAPA for trees 10–21 in. (25.4–53.3 cm) were the most frequently selected density attributes, each appearing in 106 models. Proportion of crown area under 20 ft (6.10 m) was most frequently (for 300 models) selected as the vertical stand structure measurement. For a short-term weather metric, 81 models omitted it entirely, while 80 models included hourly fuel temperature. For climate, 340 models included 30-year mean maximum annual temperature, with the remaining 9 omitting a climate metric. All of the top 349 models incorporated hourly maximum wind gust speed (hr_spd_maxgust). Finally, of the possible combinations of unrestricted variables, basal area of standing dead wood as the only unrestricted variable was the most common outcome, appearing in 80 of the top models.

Averaged model

The averaged model incorporates all 24 variables except for daily windspeed and 30-year mean precipitation, neither of which appear in the set of models with ΔAICc < 7. The estimated coefficient for hourly windspeed has the greatest magnitude, followed by the proportion of canopy area below 20 ft (6.10 m), 30-year maximum temperature, basal area of standing dead wood, and BAPA for trees between 10 and 21 in. (25.4–53.3 cm) (Table 2; Fig. 7). Because all variables were scaled and centered to have a mean of 0 and a standard deviation of 1, parameter magnitudes can be interpreted relative to changes of one standard deviation in their respective variable (listed in Table S1) (Menard 2011).

The averaged model has an AUC of 0.727, whereas we would expect an AUC of 0.5 for the null model (i.e., one in

Fig. 7. Coefficients and 95% confidence intervals on parameters in the multi-model average calculated from models with ΔAICc < 7. Coefficients are based on scaled and centered variables, and represent the mean parameter value across all models, weighted by Akaike weight. BAPA, basal area per acre; AICc, corrected Akaike information criterion.

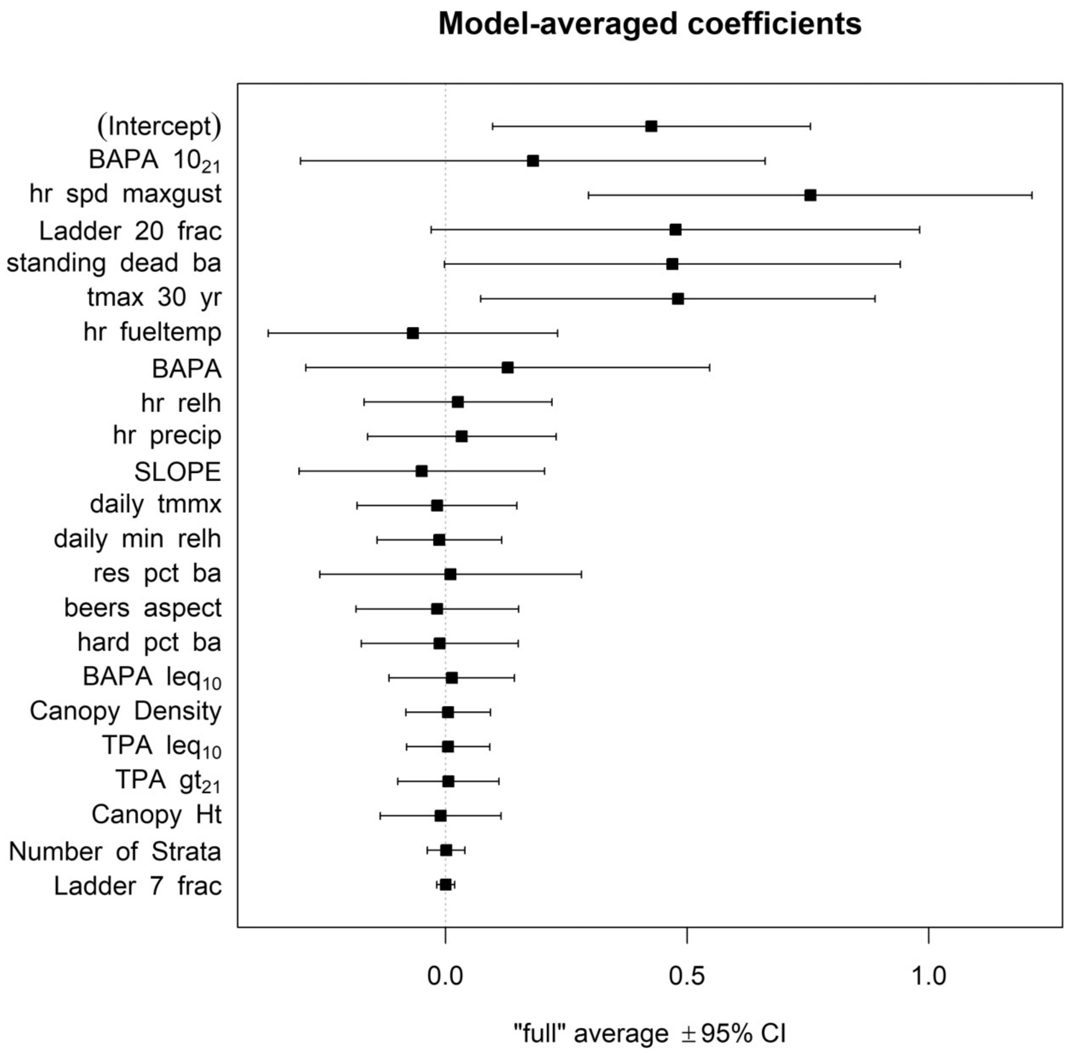

which severity is predicted randomly). When predictions are binned using a breakpoint of 0.5, the model correctly classifies the burn severity of FIA plots in the validation fold on average 63.6% of the time, with a Cohen's kappa statistic of 0.24. This indicates better performance than the null model (associated with Cohen's kappa of 0) but far from perfect agreement (associated with Cohen's kappa of 1) (Fig. 8; Table 3). The spatial correlogram developed from residuals clusters near the *x*-axis, indicates a low degree of spatial autocorrelation for all tested neighborhood ranges (Fig. S2), making unlikely the omission of an important, spatially defined predictor (Legendre and Fortin 1989).

Mapping

When applied to imputed stand structure, estimated weather, and climate for each forested 30 m pixel on national forest or national park land within the Dixie footprint, the three tested models had a maximum AUC of 0.54. At a classification threshold of 0.5, pixels were correctly classified at most 55.2% of the time, and the highest Cohen's kappa was 0.042, only slightly higher than the level of agreement expected from the null model. Applying the burn severity prediction model to currently available, spatially comprehensive representations of the model inputs does not produce a map reliable enough to serve as the basis for management decisions. Mapped residuals exhibited a high degree of spatial clustering, with global Moran's I values ranging from 0.780 to 0.781, indicating the possibility that at pixel scale an unaccounted-for spatially autocorrelated variable (or error in the imputed predictors) is limiting model fit (Table 4; Fig. 9) (Legendre and Fortin 1989).

When the maps of predicted high burn severity likelihood were down-sampled to 65 ha cells (roughly a quarter section) based on the findings of Bell et al. (2018), the models achieved at most a 55.9% accuracy rate, with an AUC of 0.55 and Cohen's kappa of 0.078. Residual spatial autocorrelation was reduced (0.412–0.424) but remained high (Table 4).

Table 3. Confusion matrix for multi-model average.

	Actual–not severe	Actual–severe
Predicted–nonsevere	20.9%	15.5%
Predicted–severe	20.8%	42.8%

Fig. 8. Receiver operating curve for the multi-model average. This plot depicts the true positive rate plotted against the false positive rate at different classification cutoff points for assigning high burn severity to Forest Inventory and Analysis plots based on the numerical output of the logit link. A corresponding curve for the null model would be a diagonal line through the origin; larger area under the curve indicates a better ability to discriminate between categories. AUC, area under the receiver operating curve.

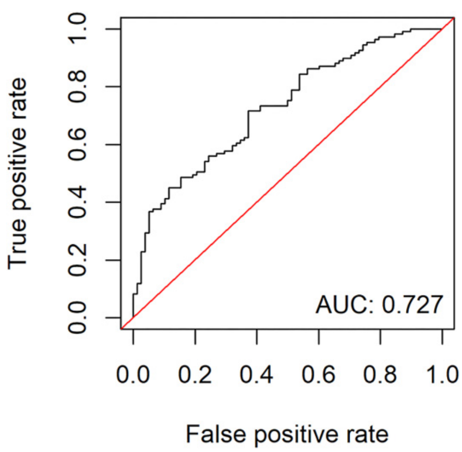

Applying the same 5-parameter model to randomly sampled LEMMA pixels and randomized basal area, standing dead wood, and ladder fuel data yielded the same AUC: 0.57. Thus, the model fit to imputed data is at least consistent with what could be expected from purely random ladder fuel and snag estimates and highly inaccurate estimates of mid-sized basal area.

To illustrate the kind of policy-relevant maps that might be produced if spatially comprehensive input data of sufficient quality were available, we generated maps of the 5-parameter model applied to the entirety of the forested areas within Lassen and Plumas National Forests and Lassen Volcanic National Park for low, moderately high, and extreme wind gust speed scenarios (Fig. S3).

Discussion

Stand density, snag density, and ladder fuels are the primary modifiable drivers of high burn severity

Our model results underscore the influence of pre-fire stand density (as measured by live tree BAPA) on burn severity as assessed via remote sensing derived indices in northern CA forests. This is consistent with findings elsewhere, for example, Amato et al. (2013) found a strong positive relationship between stand density and burn severity, as indicated by CBI, in a central New Mexico ponderosa pine forest. Walker et al. (2021) reported that both depth of burn in the organic soil layers and total C combusted increased with pre-fire conifer density. In the southern Sierra Nevada of California, Stephens et al. (2022) found that stand density and dead biomass density had the greatest influence on fire severity. Thanks to their lower moisture content and being intermingled with live trees, abundant standing dead trees may have acted to both directly ignite canopy fuels and exacerbate crown scorch as they burned, and to have generated fine and coarse down wood in the years before the Dixie fire that could have produced greater surface flame lengths and incidence of crown fire initiation that increases the odds of high burn severity outcomes. Parks et al. (2018) inferred that low-severity fires that attenuate the emergence of ladder fuels enhance resistance to stand-replacing fire. Such findings suggest that thinning and removal of especially understory trees and snags in excess of what may be needed to achieve habitat objectives could reduce the incidence of high burn severity, contingent on the weather driving fires that arrive at a forest stand.

Our model selection results also indicate that ladder fuel abundance, manifest as Ladder_20_frac–the proportion of canopy cross-sectional area belonging to trees containing live foliage positioned <20 ft (6.1 m) above the ground—may more accurately predict high burn severity than other commonly relied upon measures of vertical crown structure. Judged in terms of both the magnitude of the averaged parameter and the sum of Akaike weights, Ladder_20_frac clearly outperforms the other methods of quantifying vertical canopy structure (Table 2). Live canopy closer than 20 ft (6.1 m) to the ground, typically associated with saplings or small pole-sized trees, constitutes "ladder fuel" that transmits fire burning primarily in surface fuels (litter, duff, down logs, grasses, forbs, and low shrubs) into the forest canopy, initiating and sustaining ignition of crown fuels that leads to stand-replacing fire.

Local weather is the key uncontrolled driver of burn severity

While stand density and ladder fuel abundance are burn severity drivers that can be mitigated via management, the other two drivers with high importance in the averaged model—local scale weather on fire arrival (wind gust speed) and climate (mean of three decades of annual local temperature maxima)—are at least as important and not feasibly controlled. It is well known that observed fire severity is mediated by climate conditions and other environmental factors occurring at regional to subcontinental scales (Parisien and Moritz 2009). Moreover, extreme weather tends to overwhelm any signal from fuels, such that fuels only matter

Table 4. Parameters and accuracy metrics for models tested on Landscape Ecology, Modeling, Mapping and Analysis imputations.

Model	Parameters	AUC	Accuracy	Kappa	Residual global Moran's I
1	BAPA, hr_spd_maxgust, hr_precip, Ladder_20_frac, standing_dead_ba, tmax_30_yr	0.54 (0.55)	55.2% (55.9%)	0.042 (0.078)	0.781 (0.412)
2	BAPA_10_21, hr_spd_maxgust, hr_precip, Ladder_20_frac, standing_dead_ba, tmax_30_yr	0.53 (0.54)	54.8% (55.2%)	0.034 (0.064)	0.780 (0.424)
3	BAPA_10_21, hr_spd_maxgust, Ladder_20_frac, standing_dead_ba, tmax_30_yr	0.53 (0.54)	55.1% (55.6%)	0.038 (0.067)	0.780 (0.422)

Note: Model 1: Highest AUC within ΔAICc < 2 set, Model 2: Second highest AUC within ΔAICc < 2 set, Model 3: Constructed using the five most important parameters identified in multi-model average. Values for the imputation to 65 ha pixels shown in parentheses. AUC, area under the receiver operating curve; BAPA, basal area per acre.

to outcomes under nonextreme weather (Busby et al. 2023). Thus, the success of fuel modifications may be largely limited to less than extreme weather conditions, which are far more prevalent than extreme ones, over time. We found that cross-temporal-scale factors are also influential—both local (hourly) weather (wind gust speed) and average climate (30-year max temperature) influenced burn severity.

Sources of uncertainty and practical considerations for predicting and mapping burn severity on large fires

Stand condition imputations

The drop in AUC seen between the burn severity prediction models identified via model selection and the maps generated from those models was not entirely surprising given our low expectations for imputation quality for two of the three stand condition variables: ladder fuels and standing dead basal area. Neither we nor the creators of the LEMMA imputations expected that a remote sensing image-based imputation at 30 m resolution would provide high accuracy representations of these fine-grained attributes given that snags are almost undetectable except at very high densities and ladder fuels are virtually unobservable by satellite-based sensors.

Applying the five-parameter model to systematically sampled LEMMA pixels and FIA plots with stand condition observations replaced (or, in the case of basal area, jittered) by random samples from a Gaussian distribution resulted in identical goodness of fit (AUC of 0.57). Since both the FIA plots and LEMMA pixels derive wind speed and climate data from the same rasters, the contribution of those variables to prediction error should be roughly equivalent. We would thus expect a high-quality stand structure imputation to outperform randomized data. The fact that it did not is consistent with our suppositions about the reliability of LEMMA imputations, particularly as a basis for deriving ladder fuels and snag basal area. Further testing along these lines is needed to better understand the relative inaccuracy of each imputed variable.

FIA sampling interval

Relying on FIA plot data, with its 10-year remeasurement cycle, to represent pre-fire conditions in this analysis framework presents potential challenges for plots where the interval between the most recent pre-fire inventory and the fire date is the maximum length of 10 years. Growth and mortality over such intervals could lead to actual stand structure and composition encountered by the fire being different than the pre-fire FIA data. Although plots encountered by fire during that interval were excluded from the analysis, other disturbances such as drought, insects, or disease could also potentially change a forest plot enough to affect its resistance to stand replacing fire.

To evaluate the impact of measurement lag, we assessed volume growth, volume mortality, and percent change in volume on 53 FIA plots within a 5 km buffer around the Dixie fire perimeter that were remeasured in 2019, 2020, or 2021, as these "look-back" 10 years over the same period for which we might be concerned about significant departures. Tree volume on 41 of these had changed by less than 30% with net volume increases more common by far than declines; 9 had accumulated substantial (30–569) percentage volume increases (though typically these involved modest change to absolute volume owing to low initial volume 10 years earlier on those plots), and 3 had experienced large live volume declines (2 owing to a fire that preceded the Dixie and 1 owing to rampant mistletoe mortality). As noted earlier, plots that burned before the Dixie were excluded from our analysis dataset, so the number of plots with markedly different conditions in the worst case (10 years post-measurement) is quite small. Moreover, thanks to the availability of data from Region 5's spatially intensified plot network, 71% of plots in our analysis were measured ≤5 years before the Dixie fire. Relative to a 10-year interval, this preponderance of recent visits would reduce the differences in structure and composition between the last pre-fire FIA visit and what the fire encounters. Ongoing temporal intensification is reducing the FIA re-measurement cycle length in California from 10 years to 5 years and could lead to plot data even closer in time to a fire in most cases.

Weather at time of fire arrival

Further work is needed to improve the temporal representation of weather at all burned locations if reliable mapped predictions are needed for a fire that has already burned. Technical challenges in the production of spatially comprehensive pixel-scale representations of weather for the time fire arrived did not inspire confidence in the accuracy of this data layer. This could be one explanation for the low accu-

Fig. 9. Predicted probability of high burn severity (top left), probability of high burn severity binned using a threshold of 0.5 (top right), actual burn severity as observed by Sentinel-2 and using a cutoff defining high severity as having Relative differenced Normalized Burn Ratio > 574 (bottom left), and confusion map comparing predicted severity and actual severely burned pixels (bottom right). Private lands have been omitted from the assessment as they were not represented in the Forest Inventory and Analysis plots used to train the model. The figure was created using QGIS version 3.44.1 and assembled from the following data sources: Dixie fire boundary (CALFIRE https://gis.data.ca.gov/datasets/CALFIRE-Forestry::california-fire-perimeters-all-1/explore), Sentinel-2 derived burn severity (European Space Agency). Base map from 3D Elevation Program, courtesy of US Geological Survey.

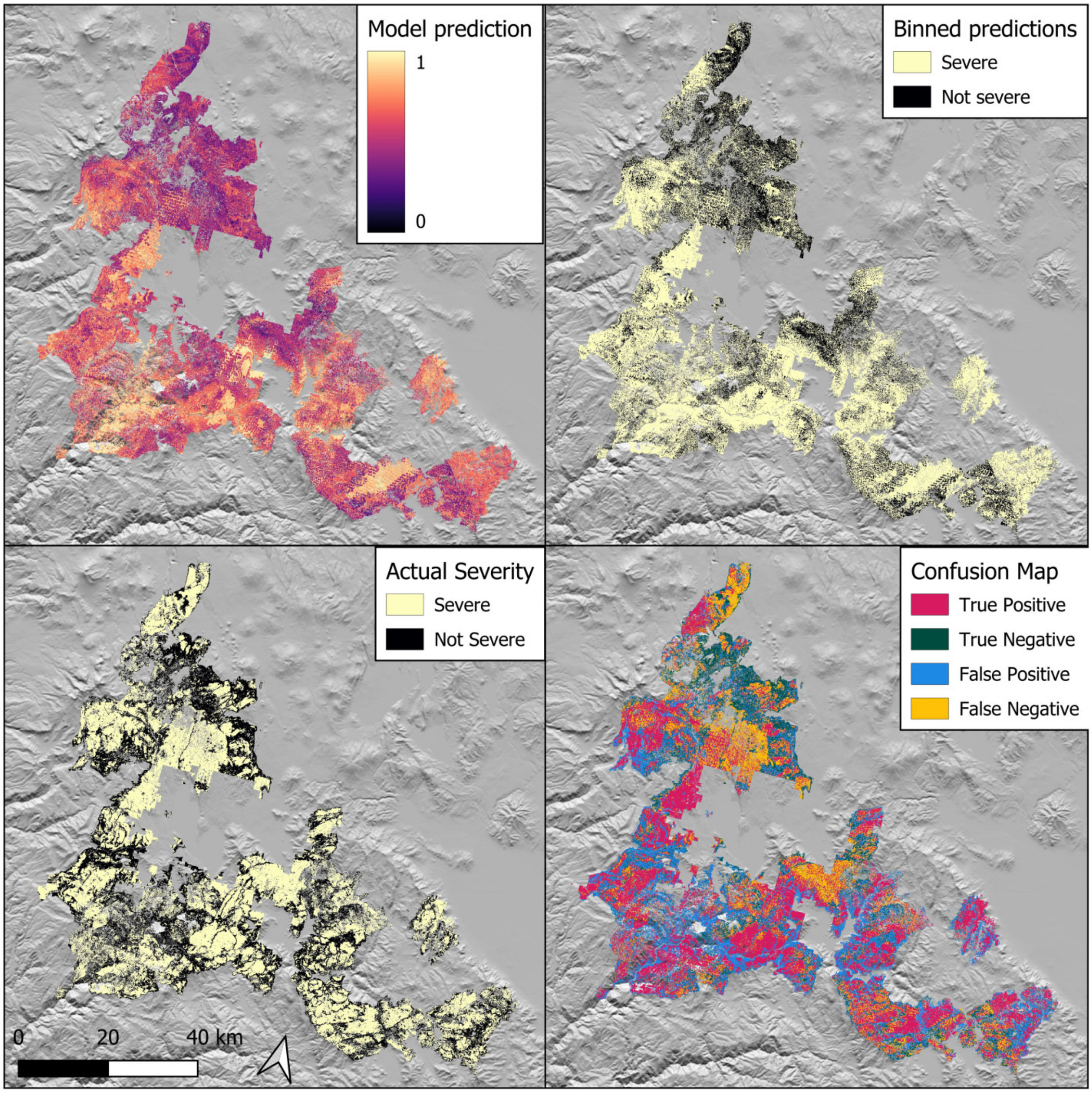

racy and residual autocorrelation evident in the confusion map (Fig. 8). Even for the far more limited number of locations occupied by the FIA plots, obtaining reliable weather estimates for the time of fire arrival was challenging. Thus, the predictions from our selected model are limited largely due to (1) uncertainty regarding fire arrival times (for plots and pixels) owing to the coarse spatial and temporal resolution obtainable from space-borne sensors and issues with data quality, temporal resolution, and availability of data derived from airborne sensors; (2) uncertainty about local weather at each plot due to RAWS spacing and topographic variation which would have required sophisticated meso-scale meteorological modeling to produce somewhat more accurate representations. To mitigate these limitations, Mass et al. (2021) and Klock et al. (2023) present methods for using Weather Research and Forecasting models to inform burn perimeter interpolation and estimate more temporally resolved local wind speed.

Prospects for improving mapped predictions

If prediction accuracy issues are traceable to inaccurate representation of weather when fire arrived, predicted severity (both probability of high burn severity, in Fig. 9, and area where high burn severity is favored by better than even odds) may prove useful to managers of an ongoing fire or pre-fire fuels planners. These predictive products could be consulted while factoring in anticipated weather or resistance goals framed with respect to weather. Alternatively, if prediction accuracy is constrained by inaccuracies in the imputation of stand structure variables, other choices are available. The LEMMA map is one of several imputed inventory-informed products already or soon to be available (others include BIGMAP and TREEMAP), and active efforts to improve the accuracy of such products are continuing. These may yet produce imputations of sufficient quality to generate better predictions from models like the one presented here. Light Detection and Ranging, in particular, can improve the measurement of ladder fuels, a known weakness in imputations relying on satellite-based sensors (Kramer et al. 2014). Moreover, it may be possible to build models for individual predictors that produce more accurate representations than can be achieved with single or multiple nearest neighbor imputations, a prospect worthy of further study. Finally, some prediction error may be attributable to inherent limitations in the relationship between remotely sensed burn severity metrics and ground-based measurements of burn severity, which we have not even begun to address here but which have been reported, for example, by Busby et al. (2023).

Implications for management

The modeling findings about the modifiable precursors to high burn severity tend to support the currently proposed silvicultural strategies for enhancing resistance to stand-replacing fire in these forests: (1) increased thinning at regular intervals to achieve and maintain the lower stand densities that historically limited the incidence of stand-replacing fire and to reduce the accrual of dead tree density beyond what is required to foster quality habitat; and (2) regular removal of ladder fuels, by hand-thinning and pruning, if required (Agee and Skinner 2005; Safford et al. 2012; Loverin et al. 2024). Given the dominating influence of wind on burn severity, local knowledge of where high wind speeds can be expected (perhaps developed from other models or experience with how weather events are concentrated by topographic features) could also contribute to the prioritization necessary to ensure that investments in fuel treatments are focused where they are likely to be effective under the wind speeds likely to be encountered (Keeley and Syphard 2019; Prichard et al. 2020). Where managers require prospective burn severity maps to prioritize and craft silvicultural operations that reduce density and ladder fuels, burn severity models such as those we constructed for the Dixie fire can be translated into wind-contingent burn severity maps (Fig. S3), provided that accurate, spatially comprehensive geodata inputs of a few key stand structure metrics, and weather and climate attributes can be developed to feed such workflows.

Conclusions

Our study of a megafire in northern California found five influential predictors of high burn severity in a multi-model average of logistic regression models: maximum hourly wind gust speed, ladder fuels, basal area of mid-sized trees, basal area of snags, and mean maximum annual temperature. The multi-model average consistently predicts burn severity (AUC of 0.727, Cohen's Kappa statistic of 0.24). Our approach shows that logistic regression models fitted to moderate-resolution imagery, systematic forest monitoring data from FIA, and imputed stand characteristics offer good prospects for mapping likelihood of high severity fire outcomes. Silvicultural treatments that reduce stand density, standing dead trees, and ladder fuels, three of the five predictor categories in our model of burn severity, enhance resistance to stand-replacing fire, contingent on local mean temperature, and wind gust speed. While more research is needed to fully understand the potential interactions among control drivers for future megafire occurrence over large areas, our results can contextualize sustainable forest management planning to ultimately reduce the incidence of large patches of stand-replacing wildfire in western United States forests.

Acknowledgements

We thank the USDA Forest Service, Pacific Southwest Research Station for project funding (Joint Venture Agreement No. 19-JV-11272139-025). We would also like to acknowledge the USDA Forest Service Pacific Northwest Research Station's Forest Inventory and Analysis Program and its spatial data services coordinator John Chase for providing access to exact plot coordinates through an Agreement (#23-RD-11261979-006). We thank Kaelyn Finlay for her assistance in acquiring hourly weather and fire progression data, Vicente Monleon, Sebastian Busby, and Nicholas Povak for their advice on developing the paper, and Matt Gregory for his assistance obtaining and understanding LEMMA data. We also thank John Loverin, whose master's thesis *Assessing Resilience of Forests to Wildfires and Fuel Management in Northern California through Forest Inventory and Aerial Photography Analyses* inspired the original form of this project.

Article information

History dates
Received: 25 November 2024
Accepted: 17 July 2025
Version of record online: 9 October 2025

Data availability
FIA Data with "fuzzed" coordinates are available at https://apps.fs.usda.gov/fia/datamart/datamart.html. Sentinel-2 imagery data are available at https://scihub.copernicus.eu/. The 2021 Visible Infrared Imaging Radiometer Suite (VI-

IRS) Suomi NPP Active Fire product from NASA FIRMS at https://www.earthdata.nasa.gov/learn/find-data/near-real-time/viirs; gridMET can be download at https://www.climatologylab.org/gridmet.html. Weather stations RAWS data are available at https://raws.dri.edu/. LEMMA imputation maps are available at https://lemma.forestry.oregonstate.edu/.

Author information

Author ORCIDs

Thomas Estabrook https://orcid.org/0000-0002-1623-2493
Jeremy Fried https://orcid.org/0000-0003-1090-5121
Weimin Xi https://orcid.org/0000-0002-2827-8851
Haibin Su ttps://orcid.org/0000-0002-3645-2047
Jianwei Zhang https://orcid.org/0000-0003-3492-2356

Author notes

Present address for Thomas Estabrook is United States Department of Agriculture Forest Service, Pacific Northwest Research Station, Wenatchee, WA 98801, USA.

Author contributions

Conceptualization: TE, JF, WX, JZ, HS
Data curation: TE, JF, JZ, WX
Formal analysis: TE
Funding acquisition: JZ, WX, HS
Investigation: TE, JF, JZ, WX
Methodology: TE, JF, WX, JZ
Project administration: JZ, WX, JF
Resources: TE, JF, WX, JZ
Supervision: WX, JF, JZ
Validation: TE, JF
Visualization: TE, JZ
Writing – original draft: TE, JF, JZ, WX
Writing – review & editing: TE, JF, WX, JZ

Competing interests

The authors declare there are no competing interests.

Funding information

This research was supported by USDA Forest Service, Pacific Southwest Research Station Joint Venture Agreement No. 19-JV-11272139-025.

Supplementary material

Supplementary data are available with the article at https://doi.org/10.1139/cjfr-2024-0305.

References

Abatzoglou, J.T. 2013. Development of gridded surface meteorological data for ecological applications and modelling. Int. J. Climatol. **33**(1): 121–131. doi:10.1002/joc.3413.

Agee, J.K., and Skinner, C.N. 2005. Basic principles of forest fuel reduction treatments. For. Ecol. Manage. **211**: 83–96. doi:10.1016/j.foreco.2005.01.034.

Amato, V.J.W., Lightfoot, D., Stropki, C., and Pease, M. 2013. Relationships between tree stand density and burn severity as measured by the Composite Burn Index following a ponderosa pine forest wildfire in the American Southwest. For. Ecol. Manage. **302**: 71–84. doi:10.1016/j.foreco.2013.03.015.

Anderson, D., and Burnham, K. 2004. Model selection and multi-model inference. Vol. 63. 2nd ed. Springer-Verlag, NY.

Azuma, D.L. 2004. Southwest Oregon biscuit fire: an analysis of forest resources and fire severity. No. 560. US Department of Agriculture, Forest Service, Pacific Northwest Research Station.

Background, Products & Applications | BAER. 2025. Usgs.gov. 2025. Available from https://burnseverity.cr.usgs.gov/baer/background-products-applications [accessed 11 June 2025].

Background, Products & Applications | RAVG. 2016. Usgs.gov. 2016. Available from https://burnseverity.cr.usgs.gov/ravg/background-products-applications [accessed 11 June 2025].

Barbour, M.G., and Major, J. 1988. Terrestrial vegetation of California: new expanded edition. Special publication 9. California Native Plant Society, Sacramento. 1030pp.

Barker, J.S., Fried, J.S., and Gray, A.N. 2019. Evaluating model predictions of fire induced tree mortality using wildfire-affected forest inventory measurements. Forests, **10**(11): 958. doi:10.3390/f10110958.

Barker, J.S., Gray, A.N., and Fried, J.S. 2022. The effects of crown scorch on post-fire delayed mortality are modified by drought exposure in California (USA). Fire, **5**(1): 21. doi:10.3390/fire5010021.

Bartoń, K. 2025. MuMIn: multi-model inference. R package version 1.48.11. Available from https://CRAN.R-project.org/package=MuMIn [accessed 8 June 2025].

Beaty, R.M., and Taylor, A.H. 2008. Fire history and the structure and dynamics of a mixed conifer forest landscape in the northern Sierra Nevada, Lake Tahoe Basin, California, USA. For. Ecol. Manage. **255**(3–4): 707–719. doi:10.1016/j.foreco.2007.09.044.

Bechtold, W.A., and Patterson, P.L. 2005. The enhanced Forest Inventory and Analysis program–national sampling design and estimation procedures. No. 80. USDA Forest Service, Southern Research Station.

Beers, T.W., Dress, P.E., and Wensel, L.C. 1966. Aspect transformation in site productivity research. Journal of Forestry, **64**: 691–692. doi:10.1093/jof/64.10.691.

Bell, D.M., Gregory, M.J., Van Kane, J.K., Kennedy, R.E., Roberts, H.M., and Yang, Z. 2018. Multiscale divergence between Landsat-and LiDAR-based biomass mapping is related to regional variation in canopy cover and composition. Carbon Balance Manage. **13**: 1–14. doi:10.1186/s13021-018-0104-6. PMID: 29330699.

Bessie, W.C., and Johnson, E.A. 1995. The relative importance of fuels and weather on fire behavior in subalpine forests. Ecology, **76**(3): 747–762. doi:10.2307/1939341.

Bjornstad, O.N. 2022. ncf: Spatial covariance functions. R package version 1.3-2. Available from https://CRAN.R-project.org/package=ncf [accessed 9 June 2025].

Burrill, E.A., DiTommaso, A.M., Turner, J.A., Pugh, S.A., Menlove, J., Christiansen, G., et al. 2021. The Forest Inventory and Analysis database: database description and user guide version 9.0.1 for phase 2. U.S. Department of Agriculture Forest Service.

Busby, S., Klock, A., and Fried, J.S. 2023. Inventory analysis of fire effects wrought by wind-driven megafires in relation to weather and pre-fire forest structure in the Western Cascades. Fire Ecol. **19**(1): 58. doi:10.1186/s42408-023-00219-x.

Cruz, M.G., Alexander, M.E., and Wakimoto, R.H. 2003. Assessing canopy fuel stratum characteristics in crown fire prone fuel types of western North America. Int. J. Wildland Fire, **12**(1): 39–50. doi:10.1071/WF02024.

Dixon, G.E. 2002. Essential FVS: a user's guide to the forest vegetation simulator. US Department of Agriculture Forest Service, Forest Management Service Center, Fort Collins, CO, USA.

Dormann, C.F., Elith, J., Bacher, S., Buchmann, C., Carl, G., and Carré, G., 2013. Collinearity: a review of methods to deal with it and a simulation study evaluating their performance. Ecography, **36**(1): 27–46. doi:10.1111/j.1600-0587.2012.07348.x.

EARTHDATA. 2025. NRT VIIRS 375 m active fire product VNP14IMGT distributed from NASA FIRMS. Available online https://earthdata.nasa.gov/firms. doi:10.5067/FIRMS/VIIRS/VNP14IMGT_NRT.002.

Eidenshink, J., Schwind, B., Brewer, K., Zhu, Z.-L., Quayle, B., and Howard, S. 2007. A project for monitoring trends in burn severity. Fire Ecol. **3**(1): 3–21. doi:10.4996/fireecology.0301003.

Escuin, S., Navarro, R., and Fernández, P. 2008. Fire severity assessment by using NBR (Normalized Burn Ratio) and NDVI (Normalized

Difference Vegetation Index) derived from LANDSAT TM/ETM images. Int. J. Remote Sens. **29**(4): 1053–1073. doi:10.1080/01431160701281072.

Eskelson, B.N.I., and Monleon, V.J. 2018. Post-fire surface fuel dynamics in California forests across three burn severity classes. Int. J. Wildland Fire, **27**(2): 114–124. doi:10.1071/WF17148.

Eskelson, B.N.I., Monleon, V.J., and Fried, J.S. 2016. A 6 year longitudinal study of post-fire woody carbon dynamics in California's forests. Can. J. For. Res. **46**(5): 610–620. doi:10.1139/cjfr-2015-0375.

European Space Agency (ESA). 2015. Sentinel-2 user handbook.

Eyre, F.H. 1980. Forest cover types of the United States and Canada. Society of American Foresters, Washington, DC.

Furniss, T.J., Van R. Kane, A.J.L., and Lutz, J.A. 2020. Detecting tree mortality with Landsat-derived spectral indices: improving ecological accuracy by examining uncertainty. Remote Sens. Environ. **237**: 111497. doi:10.1016/j.rse.2019.111497.

Gorelick, N., Hancher, M., Dixon, M., Ilyushchenko, S., Thau, D., and Moore, R. 2017. Google Earth Engine: planetary-scale geospatial analysis for everyone. Remote Sens. Environ. **202**: 18–27. doi:10.1016/j.rse.2017.06.031.

Gray, A.N., Brandeis, T.J., Shaw, J.D., McWilliams, W., Miles, P.D., Dengler, J., et al. 2012. Forest inventory vegetation database of the United States of America. In Special volume: vegetation databases for the 21st century. Vol. 4. pp. 225–231.

Halpern, C.B., and Antos, J.A. 2022. Burn severity and pre-fire seral state interact to shape vegetation responses to fire in a young, western Cascade Range forest. For. Ecol. Manage. **507**: 120028. doi:10.1016/j.foreco.2022.120028.

Harrell, F.E. 2001. Regression modeling strategies: with applications to linear models, logistic regression, and survival analysis. Vol. 608. Springer, New York.

Harris, L., and Taylor, A.H. 2017. Previous burns and topography limit and reinforce fire severity in a large wildfire. Ecosphere, **8**(11): e02019. doi:10.1002/ecs2.2019.

Hudak, A.T., Morgan, P., Bobbitt, M.J., Smith, A.M.S., Lewis, S.A., Lentile, L.B., et al. 2007. The relationship of multispectral satellite imagery to immediate fire effects. Fire Ecol. **3**: 64–90. doi:10.4996/fireecology.0301064.

Keeley, J.E., and Syphard, A.D. 2019. Twenty-first century California, USA, wildfires: fuel-dominated vs. wind-dominated fires. Fire Ecol. **15**(1): 1–15. doi:10.1186/s42408-019-0041-0.

Keeley, J.E., Pfaff, A., and Caprio, A.C. 2021. Contrasting prescription burning and wildfires in California Sierra Nevada national parks and adjacent national forests. Int. J. Wildland Fire, **30**(4): 255–268. doi:10.1071/WF20112.

Key, C.H., and Benson, N.C. 1999. Measuring and remote sensing of burn severity. *In* Proceedings Joint Fire Science Conference and Workshop. Vol. 2. University of Idaho and International Association of Wildland Fire, Moscow, ID. p. 284.

Key, C.H., and Benson, N.C. 2006. Landscape assessment (LA). In FIREMON: Fire effects monitoring and inventory system. Gen. Tech. Rep. RMRS-GTR-164-CD. *Edited by* D. C. Lutes, Robert E. Keane, John F. Caratti, Carl H. Key, Nathan C. Benson, Steve Sutherland, and Larry J. Gangi, **Vol. 164**p. LA–L1.

Keyser, C.E. 2008. Inland California and Southern Cascades (CA) variant overview–forest vegetation simulator. US Department of Agriculture Forest Service, Fort Collins, Colorado.

Klock, A.M., Busby, S., and Fried, J.S. 2023. It's about time: a method for estimating wildfire arrival and weather conditions at field-sampled locations. Fire, **6**(9): 360. doi:10.3390/fire6090360.

Kramer, H., Collins, B., Kelly, M., and Stephens, S. 2014. Quantifying ladder fuels: a new approach using LiDAR. Forests, **5**(6): 1432–1453. doi:10.3390/f5061432.

Legendre, P., and Fortin, M.J. 1989. Spatial pattern and ecological analysis. Vegetation, **80**(2): 107–138. doi:10.1007/BF00048036.

Loverin, J.K., Xi, W., Su, H., and Zhang, J. 2024. Thinning and managed burning enhance forest resilience in northeastern California. Ecosyst. Health Sustainability, **10**. doi:10.34133/ehs.0164.

Lydersen, J.M., North, M.P., and Collins, B.M. 2014. Severity of an uncharacteristically large wildfire, the Rim Fire, in forests with relatively restored frequent fire regimes. For. Ecol. Manage. **328**: 326–334. doi:10.1016/j.foreco.2014.06.005.

Mass, C.F., Ovens, D., Conrick, R., and Saltenberger, J. 2021. The September 2020 wildfires over the Pacific Northwest. Weather Forecast. **36**(5): 1843–1865. doi:10.1175/WAF-D-21-0028.1.

McLauchlan, K.K., Higuera, P.E., Miesel, J., Rogers, B.M., Schweitzer, J., Shuman, J.K., et al. 2020. Fire as a fundamental ecological process: research advances and frontiers. J. Ecol. **108**(5): 2047–2069. doi:10.1111/1365-2745.13403.

Menard, S. 2011. Standards for standardized logistic regression coefficients. Soc. Forces, **89**(4): 1409–1428. doi:10.1093/sf/89.4.1409.

Miller, J.D., and Thode, A.E. 2007. Quantifying burn severity in a heterogeneous landscape with a relative version of the delta Normalized Burn Ratio (dNBR). Remote Sens. Environ. **109**(1): 66–80. doi:10.1016/j.rse.2006.12.006.

Miller, J.D., Knapp, E.E., Key, C.H., Skinner, C.N., Isbell, C.J., Max Creasy, R., and Sherlock, J.W. 2009. Calibration and validation of the Relative differenced Normalized Burn Ratio (RdNBR) to three measures of fire severity in the Sierra Nevada and Klamath Mountains, California, USA. Remote Sens. Environ. **113**(3): 645–656. doi:10.1016/j.rse.2008.11.009.

Miller, M.E., Billmire, M., Elliot, W.J., Endsley, K.A., and Robichaud, P.R. 2015. Rapid response tools and datasets for post-fire modeling: linking Earth observations and process-based hydrological models to support post-fire remediation. International Archives of the Photogrammetry, Remote Sensing & Spatial Information Sciences, **XL-7(W3)**: 469–476.

Moody, T.J., Fites-Kaufman, J.A., and Stephens, S.L. 2006. Fire history and climate influences from forests in the northern Sierra Nevada. USA Fire Ecol. **2**: 115–141. doi:10.4996/fireecology.0201115.

MTBS Data Access: Fire Level Geospatial Data. 2017. MTBS project. USDA Forest Service/U.S. Geological Survey. Available from http://mtbs.gov/direct-download [accessed 28 April 2023].

North, M.P., York, R.A., Collins, B.M., Hurteau, M.D., Jones, G.M., Knapp, E.E., et al. 2021. Pyrosilviculture needed for landscape resilience of dry western United States forests. J. For. **119**(5): 520–544. doi:10.1093/jofore/fvab026.

Ohmann, J.L., Gregory, M.J., Henderson, E.B., and Roberts, H.M. 2011. Mapping gradients of community composition with nearest-neighbour imputation: extending plot data for landscape analysis. J. Veg. Sci. **22**(4): 660–676. doi:10.1111/j.1654-1103.2010.01244.x.

Parisien, M.-A., and Moritz, M.A. 2009. Environmental controls on the distribution of wildfire at multiple spatial scales. Ecol. Monogr. **79**(1): 127–154. doi:10.1890/07-1289.1.

Parks, S.A., Dobrowski, S.Z., and Panunto, M.H. 2018. What drives low-severity fire in the Southwestern USA? Forests, **9**: 165. doi:10.3390/f9040165.

Parks, S.A., Miller, C., Nelson, C.R., and Holden, Z.A. 2014. Previous fires moderate burn severity of subsequent wildland fires in two large western US wilderness areas. Ecosystems, **17**: 29–42. doi:10.1007/s10021-013-9704-x.

Pelletier, F., NI Eskelson, B., Monleon, V.J., and Tseng, Y.-C. 2021. Using Landsat imagery to assess burn severity of national forest inventory plots. Remote Sens. **13**(10): 1935. doi:10.3390/rs13101935.

Peterson, D.L. 2007. A consumer guide: tools to manage vegetation and fuels. Vol. 690. US Department of Agriculture, Forest Service, Pacific Northwest Research Station.

Prichard, S.J., Povak, N.A., Kennedy, M.C., and Peterson, D.W. 2020. Fuel treatment effectiveness in the context of landform, vegetation, and large, wind-driven wildfires. Ecol. Appl. **30**(5): e02104. doi:10.1002/eap.2104. PMID: 32086976.

PRISM Climate Group. 2014. Oregon State University. Available from https://prism.oregonstate.edu [accessed 16 December 2020].

R Core Team. 2023. R: a language and environment for statistical computing. pp. 275–286.

Reinhardt, E.D. 2003. The fire and fuels extension to the forest vegetation simulator. United States Department of Agriculture Forest Service, Rocky Mountain Research Station.

Robichaud, P.R., Lewis, S.A., Brown, R.E., and Ashmun, L.E., 2009. Emergency post-fire rehabilitation treatment effects on burned area ecology and long-term restoration. Fire Ecol. **5**: 115–128. doi:10.4996/fireecology.0501115.

Safford, H.D., Stevens, J.T., Merriam, K., Meyer, M.D., and Latimer, A.M., 2012. Fuel treatment effectiveness in California yellow pine and mixed conifer forests. Forest Ecology and Management **274**: 17–28.

Shaw, J.D., Goeking, S.A., Menlove, J., and Werstak, C.E., Jr. 2017. Assessment of fire effects based on Forest Inventory and Analysis data and a long-term fire mapping data set. J. For. **115**(4): 258–269. doi:10.5849/jof.2016-115.

Sing, T., Sander, O., Beerenwinkel, N., and Lengauer, T. 2005. ROCR: visualizing classifier performance in R. Bioinformatics, **21**(20): 3940–3941. doi:10.1093/bioinformatics/bti623. PMID: 16096348.

Stephens, S.L., Bernal, A.A., Collins, B.M., Finney, M.A., Lautenberger, C., and Saah, D., 2022. Mass fire behavior created by extensive tree mortality and high tree density not predicted by operational fire behavior models in the southern Sierra Nevada. Forest Ecology and Management, **518**: 120258. doi:10.1016/j.foreco.2022.120258.

Stoker, J., and Miller, B. 2022. The accuracy and consistency of 3D elevation program data: a systematic analysis. Remote Sens. **14**(4): 940. doi:10.3390/rs14040940.

Taylor, A.H., Harris, L.B., and Drury, S.A. 2021. Drivers of fire severity shift as landscapes transition to an active fire regime, Klamath Mountains, USA. Ecosphere, **12**(9): e03734. doi:10.1002/ecs2.3734.

Taylor, A.H., Harris, L.B., and Skinner, C.N. 2022. Severity patterns of the 2021 Dixie fire exemplify the need to increase low-severity fire treatments in California's forests. Environ. Res. Lett. **17**(7): 071002. doi:10.1088/1748-9326/ac7735.

Tinkham, W.T., Mahoney, P.R., Hudak, A.T., Domke, G.M., Falkowski, M.J., Woodall, C.W., and Smith, A.M.S. 2018. Applications of the United States Forest Inventory and Analysis dataset: a review and future directions. Can. J. For. Res. **48**(11): 1251–1268. doi:10.1139/cjfr-2018-0196.

Turco, M., Abatzoglou, J.T., Herrera, S., Zhuang, Y., Jerez, S., Lucas, D.D., et al. 2023. Anthropogenic climate change impacts exacerbate summer forest fires in California. Proc. Natl. Acad. Sci. USA, **120**(25): e2213815120. doi:10.1073/pnas.2213815120.

Tyukavina, A., Potapov, P., Hansen, M.C., Pickens, A.H., Stehman, S.V., Turubanova, S., Parker, D., et al. 2022. Global trends of forest loss due to fire from 2001 to 2019. Front. Remote Sens. **3**: 825190. doi:10.3389/frsen.2022.825190.

United States Department of Agriculture (USDA) Forest Service PNW Research Station FIA. 2022*c*. Field instructions for the annual inventory of California, Oregon, and Washington 2022. On file at PNW-FIA. Available from https://research.fs.usda.gov/sites/default/files/2023-02/2022_pfsl_fia_field_manual.pdf [accessed 16 September 2025].

United States Department of Agriculture (USDA) Forest Service. 2023. Confronting the wildfire crisis. *In* Wildfire Crisis Strategy FS-1187f. United States Department of Agriculture, Washington, DC.

US Forest Service. 2022a. Confronting the wildfire crisis: a chronicle from the National Fire Plan to the Wildfire Crisis Strategy. *In* Wildfire Crisis Strategy FS–1187c. United States Department of Agriculture, Washington, DC.

US Forest Service. 2022b. WCS-initial landscape investments. *In* Wildfire Crisis Strategy FS-1187d. United States Department of Agriculture, Washington, DC. Available from https://www.fs.usda.gov/sites/default/files/WCS-Initial-Landscape-Investments.pdf [accessed 26 May 2023].

Varga, K., Jones, C., Trugman, A., Carvalho, L.M.V., McLoughlin, N., Seto, D., et al. 2022. Megafires in a warming world: what wildfire risk factors led to California's largest recorded wildfire. Fire, **5**(1): 16. doi:10.3390/fire5010016.

Walker, X.J., Howard, B.K., Jean, M., Johnstone, J.F., Roland, C., Rogers, BM., et al. 2021. Impacts of pre-fire conifer density and wildfire severity on ecosystem structure and function at the forest-tundra ecotone. PLoS One, **16**(10): e0258558. doi:10.1371/journal.pone.0258558. PMID: 34710129.

Williams, A.P., Abatzoglou, J.T., Gershunov, A., Guzman-Morales, J., Bishop, D.A., Balch, J.K., and Lettenmaier, D.P. 2019. Observed impacts of anthropogenic climate change on wildfire in California. Earth's Future, **7**(8): 892–910. doi:10.1029/2019EF001210.

Woo, H., NI Eskelson, B., and Monleon, V.J. 2021. Sensitivity analysis on distance-adjusted propensity score matching for wildfire effect quantification using national forest inventory data. Environ. Modell. Software, **144**: 105163.